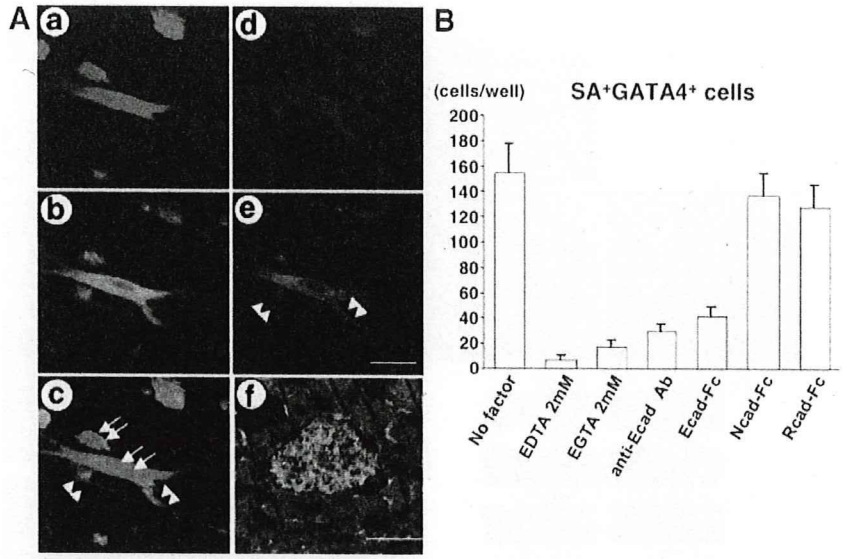

Figure 4. Differentiation of bone marrow mononuclear cells (BMMNCs) into cardiomyocytes (CMs) is mainly induced by bivalent cation-mediated cell contact with brown adipose tissue-derived cells (BATDCs). **(A):** Immunocytochemical staining of CMs from BMMNCs cocultured with fixed BATDCs for 14 days. Anti-GFP (green) (a and c), anti-SA(red) (d and e), and anti-pan-cadherin (blue) (b, c, and e) Abs were used in this assay. Arrows indicate SA^+GFP^+ cells interacting with SA^-GFP^- cells (arrowheads) through cadherin expression. f, Transmission electron micrographic analysis showed that BM-derived CMs had well-organized sarcomeres, Z-band, and a large number of mitochondria. Scale bar = 10 μm (e) and 1 μm (f). **(B):** Quantitative evaluation of differentiated CMs from BMMNCs in the presence or absence of EGTA, EDTA, or 100 μg/ml neutralizing Ab of Ecad, Ecad-Fc, Ncad-Fc, or Rcad-Fc when cocultured with fixed BATDCs. Adherent SA-positive and GATA-4-positive cells were counted in each culture condition. Results represent the mean of five independent experiments. Abbreviations: Ab, antibody; Ecad, E-cadherin; Ncad, N-cadherin; Rcad, R-cadherin.

entiated BATDCs (fixed), differentiation of BMCs into CMs was almost completely suppressed (Fig. 4B). Next, we examined which, out of E-cadherin (ECad), NCad, or RCad, was affected in this mechanism. We found that $CD133^+$ BATDCs abundantly expressed Ecad, and BMCs expressed Ecad and Ncad, as confirmed by PCR analysis (data not shown). To evaluate the effect of cadherins in this culture system, we added neutralizing antibody (Ab) against Ecad (anti-Ecad Ab) or soluble cadherin, such as Ecad-Fc, Ncad-Fc, or Rcad-Fc. Among these materials, anti-Ecad Ab and Ecad-Fc effectively inhibited the differentiation of BMMNCs into CMs. Taken together, these data suggest that Ecad-mediated cell-to-cell contact is important for the differentiation of BMMNCs into CMs.

Educated BMMNCs Contributed to CM Regeneration

The data above clearly indicate that CD133-positive BATDCs effectively induced CM production from BMCs. Next, we evaluated the length of time required for BMMNCs to become committed to CM lineage when cultured with BATDCs. For this purpose, we attempted to coculture BMMNCs from green rats expressing GFP with BATDCs for 1 to 10 days and harvested GFP-positive cells at intervals from the culture. GFP-positive cells were then sorted and cultured alone for an additional 14 days (Fig. 5A, a). In this experiment, we found that 5 days was enough for commitment of BMMNCs into CM lineage. Sorted GFP-positive cells did not express SA and GATA-4 (data not shown); however, they started to display contractile activity after 7 days of culturing. After 14 days of culturing, we found that approximately 10% of GFP-positive adherent cells differentiated into SA-positive and MEF2C-positive cells (Fig. 5A, b–d). To examine cardiac-specific genes and transcription factors in detail, we performed RT-PCR analysis and revealed that the expression of α-MHC, β-MHC, α-skeletal actin, α-cardiac actin, MLC-2v, and GATA4 was detected (Fig. 5A, e). Interestingly, this phenotype was similar to that of CMs derived from BATDCs [9].

Next, to determine whether BMMNCs exposed to BATDCs could effectively contribute to the regeneration of the heart, we injected the exposed BMMNCs into the hearts of rats after the induction of an acute MI. At first, we cocultured GFP-positive BMMNCs with CD133-positive BATDCs for 5 days, purified the GFP-positive cells by FACS, and injected the cells into the hearts of experimental MI rats at each of five sites at the border of the infarcted tissue. As a control, infarcted hearts were injected either with equal volumes and numbers of nonexposed (naive) BMMNCs or with saline. First, we revealed that donor-derived, exposed GFP-positive and SA- or ANF-positive cells were detected in abundance in the infarct border zone (Fig. 5B, a and d; 16.8% ± 2.1% of total cardiomyocytes in one field), but there were 15-fold fewer after injecting nonexposed GFP-positive cells (1.1% ± 0.4%). Hearts injected with exposed BMMNCs expressed SA-positive CMs, which also expressed connexin43 (Fig. 5B, a–c), and ANF (Fig. 5B, d–f). This indicated that transplanted BMMNCs formed gap junctions and intercalated disks and secreted CM-specific factor. Moreover, the assessment of cardiac function by echocardiography revealed that the hearts injected with exposed BMMNCs showed improved contractions of movement of the infarcted anterior walls and reduced left ventricular remodeling compared with the hearts injected with naive BMMNC or saline (Table 1). To exclude the possibilities of cell fusion in this model, we performed FISH staining with chromosome X- and Y-specific paint and revealed that educated BMMNCs (e-BMCs) implanted from male rats into female rats formed CM stained only with XY chromosome, not XXXY (Fig. 5C, a and b). This indicated that in vivo cardiac differentiation of BMMNCs was not induced by the fusion mechanism.

Nonhematopoietic Cells in the BM Are a Major Source of CM

Two candidates for the ability to regenerate myocardial tissue are HSCs and nonhematopoietic MSCs, as previously reported [1–4]. However, a recent report has indicated that the

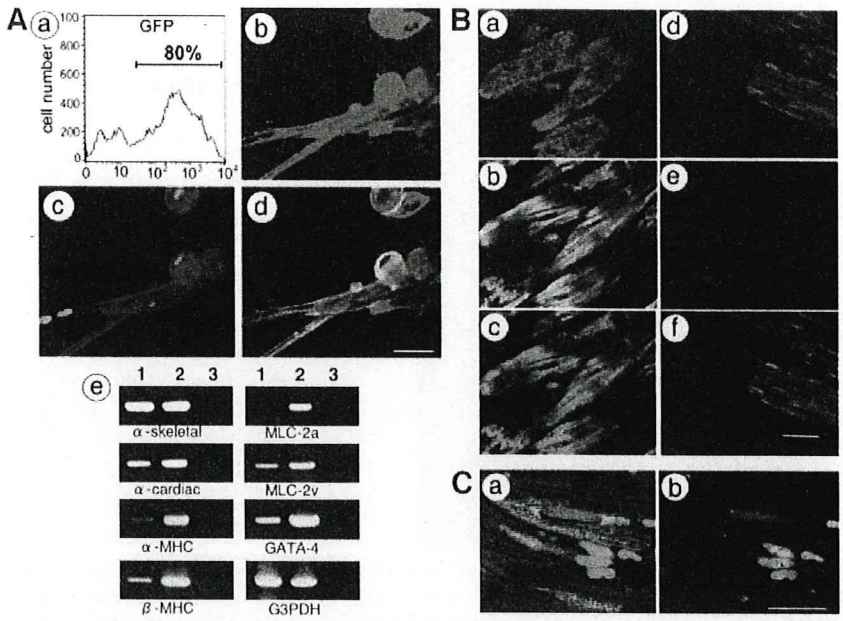

Figure 5. Bone marrow mononuclear cells (BMMNCs) cocultured with brown adipose tissue-derived cells (BATDCs) can contribute to cardiac regeneration. **(A):** Phenotype analysis of cardiomyocytes (CMs) derived from BMMNCs. a, After BMMNCs from green rats were cocultured for 5 days with BATDCs from wild-type rats, FACS analysis showed that 80% of cells were GFP-positive. b–d, Isolated GFP-positive fraction as indicated in panel a were cultured again in the absence of BATDCs for 14 days. Among adherent GFP-positive cells (green) (b), approximately 9.7% showed SA staining (red). d, MEF2C staining (blue) merged with that shown in b and c. e, Reverse transcription-polymerase chain reaction analysis of several CM-specific genes in CMs produced from BMMNCs. Lane 1, cells harvested from the conditions described in b–d (educated BMCs [e-BMCs]); lane 2, CMs from neonatal mice as a positive control; lane 3, total RNA used in lane 1 without reverse transcription. Scale bar = 5 μm. **(B):** Cells obtained as described in (A) were injected into infarcted heart, and the tissue distribution of various marker molecules was determined. a–c, GFP (green) (a), SA (blue) (b), and connexin43 (red) merged with that shown in a and b (c). d–f, GFP (green) (d), ANF (red) (e), and nuclear staining with TOPRO3 (blue) merged with that shown in d and e (f). Scale bar = 5 μm (f). **(C):** Fluorescence in situ hybridization staining in implanted site of CM. a, Section was stained with anti-SA (green) and TOPRO3 (blue). b, Serial section of panel a. Green indicates X chromosome, and red indicates Y chromosome. Nuclear staining was performed with TOPRO3 (blue). Cells expressing X and Y chromosome in the nuclei indicate that these cells were derived from e-BMCs and did not fuse with host CM expressing only X chromosome. Scale bar = 5 μm. Abbreviations: G3PDH, glyceraldehyde-3-phosphate dehydrogenase; GFP, green fluorescent protein.

Table 1. Effect of transplanted cells on myocardial performance

	Sham-operated	e-BMCs	Non-e-BMCs	Saline
Echocardiography				
Chamber diameter (mm)	6.11 ± 0.30	7.39 ± 0.70[a,b]	8.09 ± 0.77	10.8 ± 0.58
Viable WT (mm)	1.81 ± 0.17	1.71 ± 0.21[b]	1.70 ± 0.22	1.66 ± 0.13
Infarcted WT (mm)	1.80 ± 0.16	1.35 ± 0.24[a,b]	1.01 ± 0.32	0.75 ± 0.20
% Fractional shortening (%)	78.9 ± 2.1	41.9 ± 3.7[a,b]	33.1 ± 4.3	21.6 ± 2.6

The echocardiography revealed that the experimental infarct group injected with bone marrow mononuclear cells (BMMNCs) cocultured with brown adipose tissue-derived cells (BATDCs) (BMMNCs exposed to BATDCs; e-BMCs) had improved fractional shortening and reduced left ventricular internal dimension at end-diastole compared with the naïve BMMNCs (non-e-BMC)-injected group or the saline-injected group.
[a]Statistically significant difference from bone marrow ($p < .02$).
[b]Statistically significant difference from saline ($p < .01$).
Abbreviations: e-BMC, educated bone marrow cell; WT, wall thickness.

former source of CMs was generated by fusion with donor $CD45^+$ cells, suggesting that plasticity of HSC might result from the fusion of HSCs with resident cells [9]. To reveal which stem cells were capable of differentiating into CMs, we compared an HSC population and a nonhematopoietic MSC population for their ability to differentiate into CMs when cocultured with BATDCs. We sorted $Lin^-c\text{-}Kit^+$ cells and $CD45^-CD31^-CD105^+$ cells in BM from green mice, as typical of HSC and nonhematopoietic MSC populations, respectively (Fig. 6A), and then cocultured them with CD133-positive BATDCs, as shown in Figure 2B. After 14 days, cultured cells were stained with cardiac-specific antigen, which revealed that $SA^+/GATA\text{-}4^+$ cells were generated from both populations; however, the efficiency for differentiation into CMs from those two populations was quite different. As shown in Figure 6B, the number of $SA^+/GATA\text{-}4^+$ CMs from $CD45^-CD31^-CD105^+$ was over 20 times greater than that from $Lin^-c\text{-}Kit^+$ cells (Fig. 6B). These results suggested that nonhematopoietic MSCs are the major source of CMs in the BM.

DISCUSSION

Previously, we showed that BATDCs possessed cardiac progenitor cells, which contributed to the in vivo regeneration of damaged cardiac tissues [9]. Therefore, we suggested that BATDCs might be one of the prospective sources that could overcome issues associated with the regeneration of CMs. In this

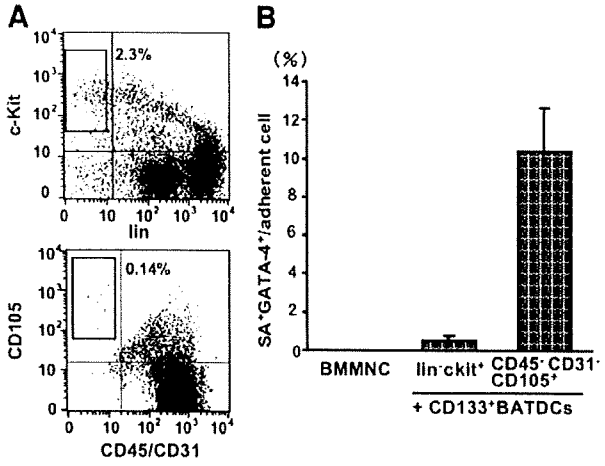

Figure 6. Nonhematopoietic MSCs in bone marrow (BM) mainly differentiate into cardiomyocytes (CMs). **(A):** Cells derived from BM were stained with anti-lineage (mixture of ter119, Mac-1, Gr-1, CD4, CD8, and B220 antibodies) marker or anti-CD31 and anti-CD45 antibodies (*x*-axis) and anti-c-Kit or anti-CD105 antibody (*y*-axis). The percentage of $lin^-c\text{-}Kit^+$ cells and $CD45^-CD31^-CD105^+$ cells in BM are indicated in the box. **(B):** Quantitative evaluation of differentiated SA- and GATA-4-positive CMs from fractionated BMMNCs, as indicated under coculturing with $CD133^+$ BATDCs. Among the adhering BM cells, 10.7% (850 ± 172) and 0.4% (23 ± 3) were SA^+/GATA-4^+ cells from $lin^-c\text{-}Kit^+$ and $CD45^-CD31^-CD105^+$ cells, respectively. BMMNCs alone did not produce CMs. Results represent the mean of five independent experiments. Abbreviations: BATDC, brown adipose tissue-derived cell; BMMNC, bone marrow mononuclear cell.

study, we looked for stem cell markers of CMs in BAT. To this purpose, we compared the capacity for differentiation into CMs from fractionated cells based on the expression levels of c-Kit, Sca-1, and CD133. We could not induce CMs from c-Kit-positive cells, and Sca-1 did not notably increase the numbers of cells that differentiated into CMs. However, there was a remarkable difference in favor of CD133-positive over CD133-negative cells in the ability to differentiate into CMs. Previous studies indicated that CD133 is a common stem cell marker, associated with, for example, neural stem cells, HSCs, endothelial progenitor cells (EPCs), epithelial stem cells, and cancer stem cells. Moreover, it was reported that EPCs differentiated into CMs upon coculturing with neonatal CMs [31]. The results from these previous studies, taken alongside those from our present study, strongly suggest that CD133 might be the CSC marker for stem cell sources in adipose and other tissues. CD133-expressing cells in BAT from the interscapular region were relatively abundant in the embryonic and neonatal stage but were reduced in the adult stage (3.5% vs. 0.2%; data not shown). Moreover, BAT does not exist in great abundance in the adult human. Therefore, BAT itself might not have a clinical application for myocardial disease in adult patients. However, using the evidence that BATDCs can differentiate into CMs and CD133-positive cells from BAT can induce BMMNCs into CMs, we might be able to investigate how BMCs can differentiate into CMs at a molecular level.

In this study, we found that when cocultured in vitro with BATDC, BMCs themselves can give rise to CMs effectively without cell fusion. In the coculture system on $CD133^+$ BATDCs, 1×10^5 total BMMNCs, which logically contained about 140 $CD45^-CD31^-CD105^+$ cells, generated 520 SA^+GATA4^+ cells. On the other hand, in the coculture of nonhematopoietic cells from BM with $CD133^+$ BATDCs, 1×10^4 $CD45^-CD31^-CD105^+$ cells generated approximately 850 SA^+GATA4^+ cells. This low efficiency of induction for CMs from $CD45^-CD31^-CD105^+$ cells may have been due to the lack of other adherent cells observed in the culture using total BMMNCs. At present, we could not determine which adherent cells from BMMNCs were important; however, macrophage and/or endothelial cells may play a role in the generation of CMs synergistically with $CD133^+$ BATDCs.

In the coculture system, when cell-to-cell contact coculture conditions were compared with this filter-separated coculture system, the former effectively induced BMCs into CMs. The culture supernatant of cultured BATDCs, even concentrated, induced BMCs into CMs with an efficiency similar to that observed in the separate coculture conditions. These results suggested that there might be two independent ways of inducing CMs from BMCs. One way is to use the fact that secreted factors determine the fate of BMCs into CMs and the other is that membrane proteins do. With respect to the latter, we suggested that cadherins may mediate this crucial cell-to-cell contact. For the physical interaction of cohering cells, cadherins regulate diverse signaling process, such as differentiation, proliferation, and migration. As previously reported, Ecad-mediated cell-cell interaction, among cells that contain primordial germ cell precursors, is essential to directing such cells to the germ cell fate [30]. In the case of CM development, there is no report showing cadherin-dependent cell commitment; however, an important role for the wnt-frizzled pathway, which is closely related to cadherin, in cardiac development was reported previously [32]. Indeed, calcium depletion with EDTA or EGTA, which prevents cadherin-mediated cell-to-cell contact, abolished the adhesion of BMMNCs to CMs. In addition, cadherins are expressed in GFP^+ BMMNC-derived cells and are localized to the sites of cell-to-cell contact between BMMNCs and BAT CMs (Fig. 4A). Among several type of cadherins, we detected that the suppression of Ecad function was effective in inhibiting both the adhesion of BMMNCs to BATDCs and their differentiation into CMs (Fig. 4B). These data suggest a potential role of Ecad in the differentiation of BMMNCs into CMs. However, additional experiments will be necessary to show the molecular mechanisms behind the cell fate decision that involve cell-to-cell contact. Moreover, regarding the possibility of the existence of a secreted factor from BATDCs for the induction of BMCs into CMs, we found that $CD133^+$ cells expressed platelet-derived growth factor (PDGF)-AB (data not shown), and BMCs expressed platelet-derived growth factor receptor α (PDGFR-α) (data not shown). To understand the contribution of the PDGF-PDGFR system, we added neutralizing antibody against PDGFR-α into the coculture of $CD133^+$ BATDCs and BMCs. Some inhibition of the differentiation from BMCs into SA^+GATA4^+ CMs was observed after 14 days of culturing (data not shown). Moreover, we found that BATDCs expressed beneficial cytokines, such as vascular endothelial growth factor (VEGF), hepatocyte growth factor (HGF), and angiopoietin-1 (data not shown). These and other, unknown factors induced the proliferation and antiapoptotic effect of e-BMCs and contributed to the effective differentiation into SA^+GATA4^+ CMs. With these data, taken together, we confirmed that there might be two processes involved in the effective induction of BMCs into CMs: a secreted protein and cell-to-cell contact mediated by a membrane-binding protein.

With the in vivo infarction model, e-BMCs effectively differentiated into CMs and improved cardiac function. In regard to this point, we found that VEGF and HGF were highly expressed by e-BMCs compared with non-e-BMCs. Moreover, approximately twice the number of $CD31^+$ ECs was observed in the transplanted region of e-BMCs compared with that of non-e-BMCs, and we also found that a small number of e-BMCs incorporated as $CD31^+$ ECs or α-smooth muscle $actin^+$ mural cells (data not shown). These results indicated that the paracrine

effect on neighboring cardiac myocytes and angiogenesis also contributed to the beneficial effects of transplantation.

Furthermore, we found no significant difference in the total number of GFP-positive cells located around the ischemic border zone between BMMNCs exposed to BATDCs (educated BMMNCs) and noneducated BMMNCs; however, SA^+/GFP^+ CMs derived from educated BMMNCs were more than 15 times more abundant in number compared with those from noneducated BMMNCs. Recently, some groups have indicated that VEGFR-2^+/VE-$cadherin^-$ primitive cells from embryonic stem cells do not contribute to vascular cells, such as ECs or SMCs. By contrast, differentiated VE-$cadherin^+$ EPCs contributed to the vascular formation as ECs [33]. These studies suggested that committed immature cells are better sources for vascular or myocardial regeneration than undirected mesodermal-derived stem cells.

In summary, we suggest that CD133-positive cells in BATDCs form an enriched stem cell population, as well as being effective inducers from MSCs in BM to CMs in vitro and in vivo. CD133-positive cells in BATDCs might prove to have potential for the regeneration of CMs.

ACKNOWLEDGMENTS

We thank Dr. M. Okabe (Osaka University, Osaka, Japan) for providing green mice and green rats and M. Sato for technical support. This study was supported in part by a grant from the Ministry of Education, Culture, Sports, Science and Technology of Japan (N.T.).

DISCLOSURE OF POTENTIAL CONFLICTS OF INTEREST

The authors indicate no potential conflicts of interest.

REFERENCES

1 Orlic D, Kajstura J, Chimenti S et al. Bone marrow cells regenerate infarcted myocardium. Nature 2001;410:701–705.
2 Jackson KA, Majka SM, Wang H et al. Regeneration of ischemic cardiac muscle and vascular endothelium by adult stem cells. J Clin Invest 2001;107:1395–1402.
3 Toma C, Pittenger MF, Cahill KS et al. Human mesenchymal stem cells differentiate to a cardiomyocyte phenotype in adult murine heart. Circulation 2002;105:93–98.
4 Makino S, Fukuda K, Miyoshi S et al. Cardiomyocytes can be generated from marrow stromal cells in vitro. J Clin Invest 1999;103:697–705.
5 Tomita S, Li RK, Weise RD et al. Autologous transplantation of bone marrow cells improves damaged heart function. Circulation 1999;100: 247–256.
6 Murry CE, Soonpaa MH, Reinecke H et al. Haematopoietic stem cells do not transdifferentiate into cardiac myocytes in myocardial infarcts. Nature 2004;428:664–668.
7 Balsam LB, Wagers AJ, Christensen JL et al. Haematopoietic stem cells adopt mature haematopoietic fates in ischaemic myocardium. Nature 2004;428:668–673.
8 Alvarez-Dolado M, Pardal R, Garcia-Verdugo JM et al. Fusion of bone-marrow-derived cells with Purkinje neurons, cardiomyocytes and hepatocytes. Nature 2003;425:968–973.
9 Yamada Y, Wang X-D, Yokoyama S-I et al. Cardiac progenitor cells in brown adipose tissue repaired damaged myocardium. Biochem Biophys Res Commun 2006;342:662–670.
10 Weigmann A, Corbeil D, Hellwing A et al. Prominin, a novel microvilli-specific polytopic membrane protein of the apical surface of epithelial cells, is targeted to plasmalemmal protrusions of non-epithelial cells. Proc Natl Acad Sci U S A 1997;94:12425–12430.
11 Yin AH, Miraglia S, Zanjani E et al. AC133, a novel marker for human hematopoietic stem and progenitor cells. Blood 1997;90:5002–5012.
12 Peichev M, Naiyer AJ, Pereira D et al. Expression of VEGFR-2 and AC133 by circulating human CD34(+) cells identifies a population of functional endothelial precursors. Blood 2000;95:952–958.
13 Uchida N, Buck DW, He D et al. Direct isolation of human central nervous system stem cells. Proc Natl Acad Sci U S A 2000;97: 14720–14725.
14 Corbeil D, Roper K, Hellwig A et al. The human AC133 hematopoietic stem cell antigen is also expressed in epithelial cells and targeted to plasm membrane protrusions. J Biol Chem 2000;275:5512–5520.
15 Richardson GD, Robson CN, Lang SH et al. CD133, a novel marker for human prostatic epithelial stem cells. J Cell Sci 2004;117:3539–3545.
16 Torrente Y, Belicchi M, Sampaolesi M et al. Human circulating AC133+ stem cells restore dystrophin expression and ameliorate function in dystrophic skeletal muscle. J Clin Invest 2004;114:182–195.
17 Maw MA, Corbeil D, Koch J et al. A frameshift mutation in prominin-(mouse)-loke 1 causes human retinal degeneration. Hum Mol Gen 2000; 9:27–34.
18 Singh SK, Hawkins C, Clarke ID et al. Identification of human brain tumour initiating cells. Nature 2004;432:396–401.
19 Yamada Y, Takakura N. Physiological pathway of differentiation of hematopoietic stem cell population into mural cells. J Exp Med 2006; 203:1055–1065.
20 Yamada Y, Takakura N, Yasue H et al. Exogenous clustered neuropilin 1 enhances vasculogenesis and angiogenesis. Blood 2001;97:1671–1678.
21 Oh H, Bradfute SB, Gallardo TD et al. Cardiac progenitor cells from adult myocardium: Homing, differentiation, and fusion after infarction. Proc Natl Acad Sci U S A 2003;100:12313–12318.
22 Moretti A, Caron L, Nakano A et al. Multipotent embryonic isl1+ progenitor cells lead to cardiac, smooth muscle, and endothelial cell diversification. Cell 2006;127:1151–1165.
23 Wu SM, Fujiwara Y, Cibulsky SM. Developmental origin of a bipotential myocardial and smooth muscle cell precursor in the mammalian heart. Cell 2006;127:1137–1150.
24 Ito T, Suzuki A, Okabe M et al. Application of bone marrow-derived stem cells in experimental nephrology. Exp Nephrol 2001;9:444–450.
25 Zuk PA, Zhu M, Ashjian P et al. Human adipose tissue is a source of multipotent stem cells. Mol Biol Cell 2002;13:4279–4295.
26 Planat-Bénard P, Menard C, Andre M et al. Spontaneous cardiomyocyte differentiation from adipose tissue stroma cells. Circ Res 2004;94: 223–229.
27 Beltrami AP, Barlucchi L, Torella D et al. Adult cardiac stem cells are multipotent and support myocardial regeneration. Cell 2003;114: 763–776.
28 Okabe M, Ikawa M, Kominami K et al. 'Green mice' as a source of ubiquitous green cells. FEBS Lett 1997;407:313–319.
29 Terada N, Hamazaki T, Oka M et al. Bone marrow cells adopt the phenotype of other cells by spontaneous cell fusion. Nature 2002;416: 542–545.
30 Okamura D, Kimura T, Nakano T et al. Cadherin-mediated cell interaction regulates germ cell determination in mice. Development 2003;130: 6423–6430.
31 Badorff C, Brandes RP, Popp R et al. Transdifferentiation of blood-derived human adult endothelial progenitor cells into functionally active cardiomyocytes. Circulation 2003;107:1024–1032.
32 Nakamura T, Sano M, Songyang Z et al. A Wnt-and beta-catenin-dependent pathway for mammalian cardiac myogenesis. Proc Natl Acad Sci U S A 2003;100:5834–5829.
33 Sone M, Itoh H, Yamashita J et al. Different differentiation kinetics of vascular progenitor cells in primate and mouse embryonic stem cell. Circulation 2003;107:2085–2088.


See www.StemCells.com for supplemental material available online.

Available online at www.sciencedirect.com
ScienceDirect
Biochemical and Biophysical Research Communications 353 (2007) 182–188
BBRC
www.elsevier.com/locate/ybbrc

A novel approach for myocardial regeneration with educated cord blood cells cocultured with cells from brown adipose tissue

Yoshihiro Yamada [a,*], Shin-ichiro Yokoyama [b], Noboru Fukuda [b], Hiroyasu Kidoya [a], Xiao-Yong Huang [a], Hisamichi Naitoh [a], Naoyuki Satoh [a], Nobuyuki Takakura [a,*]

[a] *Department of Signal Transduction, Research Institute for Microbial Diseases, Osaka University, 3-1 Yamadaoka, Suita-shi, 565-0871, Japan*
[b] *Second Department of Internal Medicine, Nihon University School of Medicine, Ooyaguchi-kami 30-1, Itabashi-ku, Tokyo 173-8610, Japan*

Received 22 November 2006
Available online 11 December 2006

Abstract

Umbilical cord blood (CB) is a promising source for regeneration therapy in humans. Recently, it was shown that CB was a source of mesenchymal stem cells as well as hematopoietic stem cells, and further that the mesenchymal stem cells could differentiate into a number of cells types of mesenchymal lineage, such as cardiomyocytes (CMs), osteocytes, chondrocytes, and fat cells. Previously, we reported that brown adipose tissue derived cells (BATDCs) differentiated into CMs and these CMs could adapt functionally to repair regions of myocardial infarction. In this study, we examined whether CB mononuclear cells (CBMNCs) could effectively differentiate into CMs by coculturing them with BATDCs and determined which population among CBMNCs differentiated into CMs. The results show that BATDCs effectively induced CBMNCs that were non-hematopoietic stem cells (HSCs) (educated CB cells: e-CBCs) into CMs in vitro. E-CBCs reconstituted infarcted myocardium more effectively than non-educated CBMNCs or CD34-positive HSCs. Moreover, we found that e-CBCs after 3 days coculturing with BATDCs induced the most effective regeneration for impaired CMs. This suggests that e-CBCs have a high potential to differentiate into CMs and that adequate timing of transplantation supports a high efficiency for CM regeneration. This strategy might be a promising therapy for human cardiac disease.

Keywords: Stem cell; Cord blood; Adipose tissue; Myocardial regeneration; Cell fusion

Myocardial regeneration is currently a popular topic in cardiac medicine, and research in regenerative medicine has advanced in an explosive manner. Many cell types such as bone marrow mesenchymal stem cells (BM-MSCs) [1–3], embryonic stem (ES) cells [4,5], and cardiac tissue stem cells [6,7] have been found to undergo myocardial differentiation and can be used as a source for cardiomyocytes (CMs). Additional cell types may also prove to have cardiac differentiation ability. With regard to human therapy, umbilical cord blood (CB) is a promising source because transplantation of CB has already been established for patients with blood diseases. Moreover, usage of CB overcomes considerable problems encountered with other sources of CMs, such as allergenic, ethical, and tumorigenic issues. Furthermore, CB contains both hematopoietic stem cells (HSCs) [8] and MSCs [9]. Also, stem cells are more abundant in CB than in adult human peripheral blood or bone marrow (BM) and stem cells in CB have a higher proliferative potential associated with an extended life span and longer telomeres [10–12].

Indeed, $CD34^+$ cells derived from human CB homed to infarcted hearts and reduced the size of the infarcted area; this was not through direct differentiation into CMs, but through enhancing neovascularization [13,14]. These studies showed no evidence of myocytes of human origin in the infracted myocardium; however, it was reported that unrestricted somatic stem cells (USSCs) from human CB could differentiate into CMs in vitro and in vivo [15]. Such

* Corresponding authors. Fax: +81 6 6879 8314.
E-mail addresses: yamaday@biken.osaka-u.ac.jp (Y. Yamada), ntakaku@biken.osaka-u.ac.jp (N. Takakura).

0006-291X/$ - see front matter © 2006 Elsevier Inc. All rights reserved.
doi:10.1016/j.bbrc.2006.12.017

USSCs are fibroblastic in appearance and negative for hematopoietic cell markers, such as c-kit, CD34, and CD45. USSCs injected into immunosuppressed pig model of myocardial infarction (MI) improved perfusion and wall motion, reduced infarct scar size, and enhanced cardiac function. USSCs seem to be a useful source for myocardial regeneration; however, they are a rare population, therefore, expansion of USSCs is required for application to clinical therapy. In spite of these challenges for the repair of CM, to date, no clinical studies of CB have been reported. Previously, we reported that brown adipose tissue derived cells (BATDCs) included cardiac progenitor cells and they effectively differentiated into CMs in vitro and in vivo [16]. This indicated that our culture system of BATDCs contained differentiation molecular cues for CMs. When BATDCs were injected into MI rats, they differentiated into CMs as well as endothelial cells (ECs) and smooth muscle cells (SMCs), supported the growth of resident cells and vascular cells, and restored cardiac function. This suggested a potential therapeutic use for BATDCs in human ischemic heart disease. However, in humans, BAT exists only in the embryonic stage and infants, therefore, it is difficult to obtain BATDCs to treat adult cardiac disease. In this study, we examined whether mononuclear cells from CB can differentiate into CMs upon coculturing with BATDCs. Moreover, usefulness of CB cells that were exposed to BATDCs for MI repair was evaluated.

Materials and methods

Cell preparation and flow cytometry. Brown adipose tissue (BAT) was dissected from postnatal day (P1) to P7 neonates of C57BL/6 mice. BAT was dissociated by DispaseII (Roche, Mannheim, Germany), drawn through a 23G needle and prepared as single cell suspension as previously reported [16]. Human CB mononuclear cells (CBMNCs) were purchased from Cambrex (Baltimore, MD). The cell-staining procedure for the flow cytometry was also as previously described [17]. The monoclonal antibodies (mAbs) used in immunofluorescence staining were anti-human CD45, -34, and -HLA–ABC mAbs (Pharmingen, SanDiego, CA). All mAbs were purified and conjugated with fluorescein isothiocyanate (FITC), PE (phycoerythrin), biotin or allophycocyanin (APC). Biotinylated antibodies were visualized with PE-conjugated streptavidin (Pharmingen) or APC-conjugated streptavidin (Pharmingen). Cells were incubated for 5 min on ice with CD16/32 (FcγIII/II Receptor) (1:100) (Fcblock™, Pharmingen) prior to staining with primary antibody. Cells were incubated in 5% fetal calf serum/phosphate-buffered saline (FCS/PBS; washing buffer) with primary antibody for 30 min on ice, and washed twice with washing buffer. Secondary antibody was added and the cells were incubated for 30 min on ice. After incubation, cells were washed twice with, and suspended in, the washing buffer for fluorescence-activated cell sorter (FACS) analysis. The stained cells were analyzed and sorted by EPICS Flowcytometer (BECKMAN COULTER, San Jose, CA). The sorted cells were added to 24-well dishes (Nunc, Roskilde, Denmark), precoated with 0.1% gelatin (Sigma, St. Louis, USA), and cultured in Dulbecco's modified Eagle's medium (DMEM; Sigma), supplemented with 10% FCS and 10^{-5}M 2-mercaptoethanol (2-ME), at 37 °C in a 5% CO_2 incubator.

Cell coculture. BATDCs were prepared as described above. When BATDCs and human (h) CBMNCs were cocultured in contact conditions, 1×10^5 BATDCs were plated per well of a 24-well plate and cultured for 7 days, and then, 1×10^5 CBMNCs, or 1×10^4 $CD34^+$ HSCs were cultured with BATDCs for 10 days. Staining was performed with anti-cardiac troponinT (Santa Cruz), -MEF-2C (Cell signaling) and -HLA ABC antibodies (Pharmingen).

Supplemental information reveals the Materials and methods for RT-PCR analysis, Immunohistochemistry, FISH staining, and procedure for mouse myocardial infarction (MI) model and echocardiography.

Results

Differentiaion of CBMNCs into CMs by coculturing with BATDCs in vitro

Previously, we reported that BATDCs differentiate into CMs spontaneously; this suggests that BATDCs produce molecules that induce self differentiation into CMs by an autocrine loop. Moreover, CBMNCs contained cells with a potential to differentiate into various cell types, such as osteoblasts, chondrocytes, and CMs. Therefore, to determine whether molecules produced from BATDCs induce CBMNCs to differentiate into CMs effectively, we cultured CBMNCs with BATDCs and observed the differentiation of CBMNCs into CMs. At first, dissociated BATDCs from P1 to P7 neonatal mice were cultured on 0.1% gelatin-coated dishes. After 1 week, human CBMNCs were added and cocultured with BATDCs. After coculturing CBMNCs with BATDCs for 14 days, among HLA-positive CBMNCs, nuclear located MEF2C positive and cardiac troponinT-positive cells (Fig. 1A and B), or cardiac troponinI-positive cells (Fig. 1C) were effectively produced. In contrast, sorted $CD34^+38^-$HSC population from CBMNCs, which was previously reported to differentiate into CMs [18], was differentiated into cardiac troponinT-positive CMs (Fig. 1E); however, the frequency of CM differentiation from HSC population was lower than that from total CBMNCs (Fig. 1I). CBMNCs alone did not differentiate into cardiac troponinT-positive or MEF2C-positive cells spontaneously under the same culture medium without coculturing with BATDCs (Fig. 1G, H, and I).

The expression of CM-specific genes in CBMNCs educated by culturing with BATDCs

Next, we evaluated the length of time required for CBMNCs to become committed CM lineage cells when cocultured with BATDCs. For this purpose, we attempted to coculture CBMNCs with BATDCs for 1 to 7 days and $HLA^+CD45^-CD34^-$ non-hematopoietic cells [we termed them educated CB cells (e-CBCs)] were then sorted and mRNA was extracted from the cells as indicated in Fig. 2A. Because mature hematopoietic cells from cocultured CBMNCs did not differentiate into CMs (data not shown) and HSC population barely differentiated into CMs (Fig. 1), we deduced that cardiac stem/progenitor cells were more abundant in non-hematopoietic cells and were therefore $CD45^-CD34^-$. We analyzed the expression of CM-specific genes on days 0, 3, and 7 as indicated in Fig. 2B and confirmed that cardiac actin, myosin light chain 2v, and specific transcriptional factor, such as

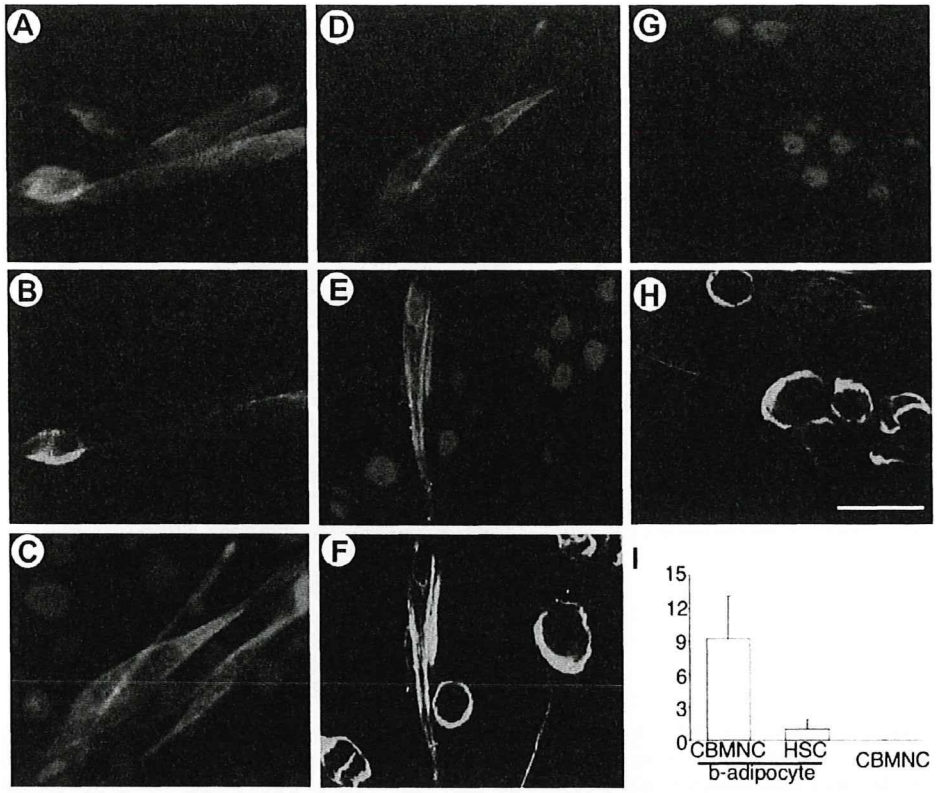

Fig. 1. CBMNCs can differentiate into CMs upon coculturing with BATDCs. Immunocytochemical analysis of human CBMNCs (A–D), and $CD34^+CD38^-$HSCs (E, F) cocultured with BATDCs from wild type mice, or CBMNCs (G, H) cultured without BATDCs for 14 days. (A) Expression of cardiac troponinT (green) and MEF2C (red). (B) Human HLA expression (blue) in the same field as (A). (C, E, and G) Expression of cardiac troponinI (green) and nuclear staining with PI (red). (D, F, and H) Human HLA expression (blue) in the same fields as (C, E, and G), respectively. Scale bar in (H) indicates 5 μm. (I) Quantitative evaluation of differentiated cardiac troponinT and MEF2C-positive CMs among adhering HLA-positive CB-derived cells. Data for CBMNC, and $CD34^+CD38^-$HSCs cocultured with BATDCs (b-adipocyte) and CBMNCs cultured without BATDCs are displayed. Results represent means ± SD of five independent experiments.

GATA-4 and Nkx2.5 were expressed on day 3 of coculture (Fig. 2B). MHC alpha and beta mRNAs were not expressed on day 3; however, they started to be expressed around day 7.

Educated CBMNCs in non-hematopoietic lineage contributed to myocardial regeneration

As indicated in Fig. 2, 3 days of coculturing with BATDCs was enough for commitment of CBMNCs into CM lineage. Next, in order to determine whether e-CBCs could effectively contribute to the regeneration of the heart, we injected the e-CBCs into the hearts of nude rats after the induction of an acute MI as indicated in Fig. 3A. At first, we cocultured CBMNCs with BATDCs for 3 days, purified $HLA^+CD45^-CD34^-$ cells (e-CBCs) by FACS and injected the cells into the hearts of experimental MI nude rats at each of five sites at the border of the infarcted tissue. As a control, infarcted hearts were injected with either equal volumes and numbers of CBMNCs that were not exposed to BATDCs (non-e-CBCs), or $CD34^+38^-$HSCs directly sorted from freshly isolated CBMNCs. Upon injection of e-CBCs, donor-derived human HLA- and SA-positive cells were detected abundantly in the infarct border zone (Fig. 3B, a, b, and c; 23.4 ± 3.1% of total cardiomyocytes in one field), but the contribution to CMs by the injection with non-e-CBCs and $CD34^+38^-$HSCs in the MI was 20- (Fig. 3B, d, e, and f; 1.1 ± 0.3%) and 15-fold (Fig. 3B, g, h, and i; 1.5 ± 0.3%), respectively, less than that of e-CBCs. e-CBC-derived SA-positive CMs also expressed connexin 43 (Fig. 3Bc), indicating that transplanted e-CBC-derived CMs formed gap junctions with host CMs. Moreover, the assessment of cardiac function by echocardiography revealed that the hearts injected with e-CBCs showed improved contractions of movement of the infarcted anterior walls and reduced left ventricular remodeling compared with the hearts injected with non-e-CBCs or $CD34^+38^-$HSCs (Fig. 4).

To clarify the origin of CMs in recipient tissue, donor-derived human chromosomes and host-derived rat chromosomes were simultaneously detected by using species-specific chromosome probes using fluorescent in situ hybridization (FISH) analysis. In this analysis, we used centromere probes, because 5 μm thick slices may not always include sex chromosomes in the nuclei as previously described [18]. Result showed that

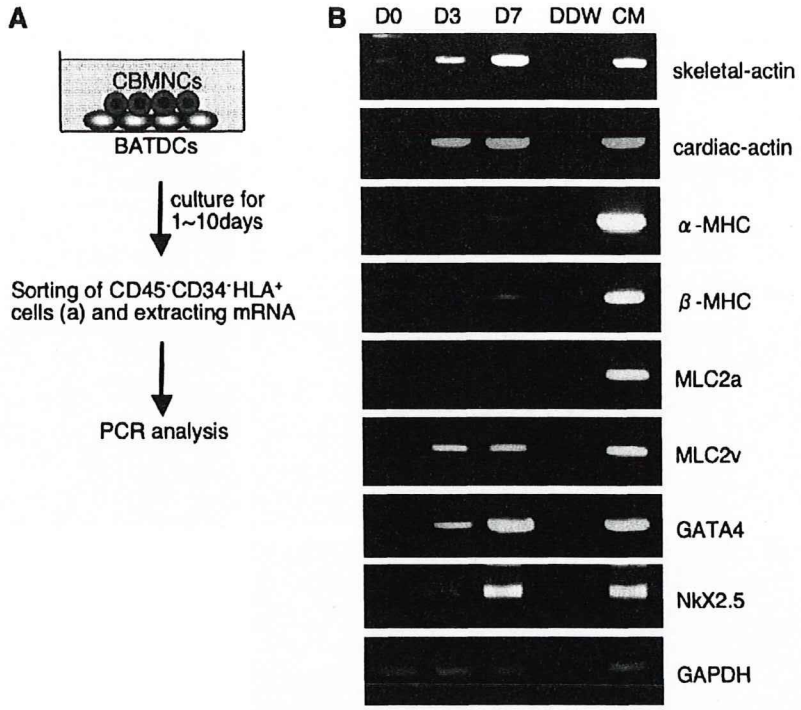

Fig. 2. Expression of CM-specific genes in e-CBCs. (A) Design of experiment for the isolation of human e-CBCs. CBMNCs were cocultured with BATDCs for 1 to 10 days, and then $CD45^{-}CD34^{-}$ human HLA^{+} cells were sorted and total RNA was extracted. (B) PCR analysis was performed with CM-specific primers in e-CBCs after coculturing with BATDCs for 0 day (D0; freshly isolated CBCs without exposure to BATDCs), 3 days (D3) and 7 days (D7). Distilled water (DDW) and CMs from embryos (CM) were used as a negative and a positive control, respectively. GAPDH was used as an internal control.

implanted e-CBCs of human origin transferred into female nude rats formed CMs that stained only with probes specific for human chromosomes (Fig. 3C, a and b). We also checked the serial confocal imaging to exclude the possibility that they arose from cell overlay as previously reported [18], but could not observe any superimposed cells (data not shown). This indicated that in vivo cardiac differentiation of e-CBCs was not induced by the fusion mechanism. In contrast, when $CD34^{+}CD38^{-}$HSCs were implanted into MI induced nude rats, human HLA-positive CMs were stained with both human and rat chromosome probes (data not shown). This indicated that generation of CM-derived HSCs was due to the fusion mechanism between donor-derived cells and host CMs as previously reported [18,19].

Discussion

So far, various kinds of sources for CMs, such as adult BM HSCs [19,20], MSCs [1–3], and ES cells [4,5] have been reported; however, there is some controversy regarding the efficiency of cardiomyoplasty. In terms of the myocardial regeneration therapy for human, human CB cells seem to be a safe and useful source compared to other sources, because these cells have already been utilized in CB transplantation for managing patients with blood disease. However, no clinical trials using CB cells to treat heart disease have been reported.

In this study, we raised two important points. The first is that e-CBCs of non-hematopoietic origin were more effectively differentiated into CMs compared with $CD34^{+}CD38^{-}$HSCs in vitro. Moreover, we showed that e-CBCs differentiation into CMs was not through the cell fusion mechanism. On the other hand, CMs derived from $CD34^{+}CD38^{-}$HSCs were generated through cell fusion with host CMs in vivo. Previously, it was reported that MSCs but not HSCs from BM could migrate into the heart and differentiate into CMs in mouse MI model [21]. This suggested that MSCs were the predominant source for myocardial regeneration. Our report is the first to show that non-hematopoietic cells can be used as CM source and how these compare with HSCs in human cord blood cells.

The second is the new strategy for myocardial regeneration using CB cells and BATDCs. Using the coculturing method described here, CB cells were effectively induced to differentiate into CMs in vitro. Moreover, e-CBCs were effectively differentiated into CMs in immunodeficient rat MI model and improved the cardiac function. Furthermore, we found that an adequate duration of coculturing of CB cells with BATDCs was critical for CM regeneration. In the present method, three days of coculturing was the most effective to produce CMs from e-CBCs and improve the CM function and this timing was consistent

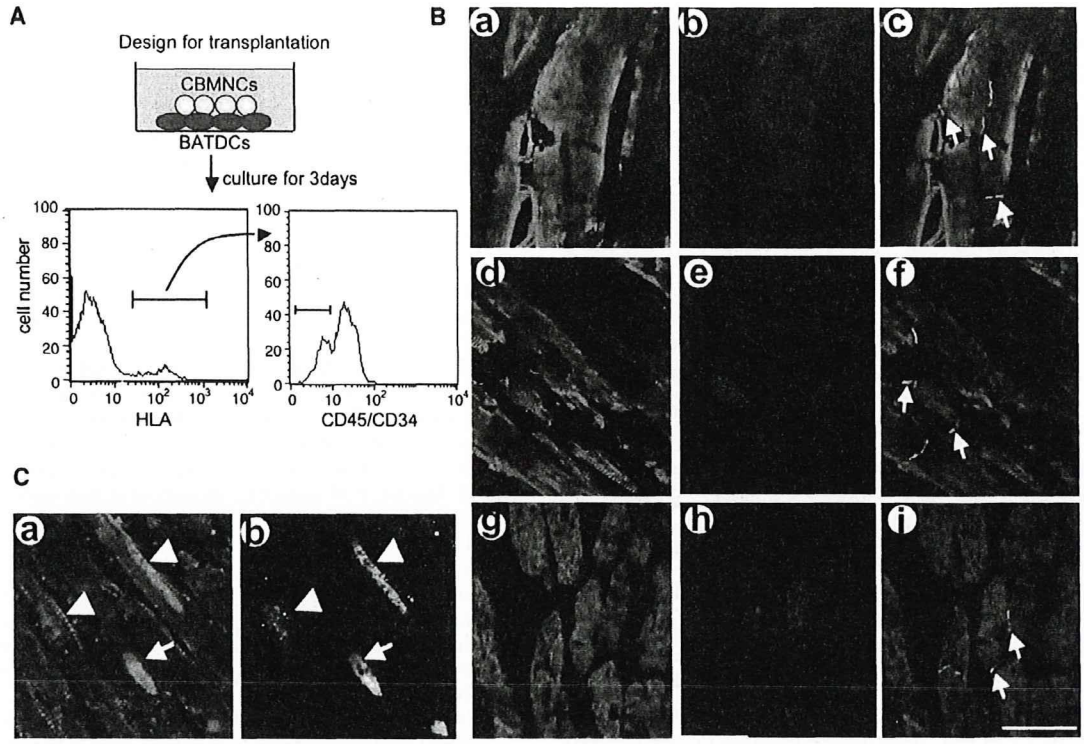

Fig. 3. CBMNCs cocultured with BATDCs contributed to cardiac regeneration. (A) Strategy for transplantation. After human CBMNCs were cocultured for 3 days with BATDCs from mice, human $HLA^+CD45^-CD34^-$ cells (e-CBCs) were sorted by FACS and injected into the border zone of ischemia induced nude rats. As a control, CBMNCs that were not cocltured (non-e-CBCs) and freshly isolated $CD34^+CD38^-$HSCs were used. (B) CM development from injected e-CBCs (a–c), non-e-CBCs (d–f), and $CD34^+CD38^-$HSCs in MI induced heart. (a, d, and g) Expression of SA (green). (b, e, and h) human HLA (red). (c, f, and i) are merged image of (a and b), (d and e), and (g and h), respectively, and stained with anti-connexin 43 antibody (blue). Arrows in (c, f, and i) indicate the regions in which human CB-derived connexin positive CMs make tight junction with resident host CMs. Scale bar in (i) indicates 20 μm. (C) (a) Expression of human HLA (red) and SA (green) in the site of implantation of e-CBCs in MI induced heart. Nuclei were counter stained with TOPRO3 (blue). (b) FISH staining in a serial section of (a). Green colors indicate rat chromosome, and red color indicates human chromosome. Nuclear staining was performed with TOPRO3 (blue). Cells expressing human chromosome (red) in the nuclei indicate that these cells were derived from e-CBCs and did not fuse with host CM expressing only rat chromosome (green). Arrowheads indicate nuclei from host CMs and arrow indicates human nuclei in e-CBCs (a, b). Scale bar indicates 5 μm.

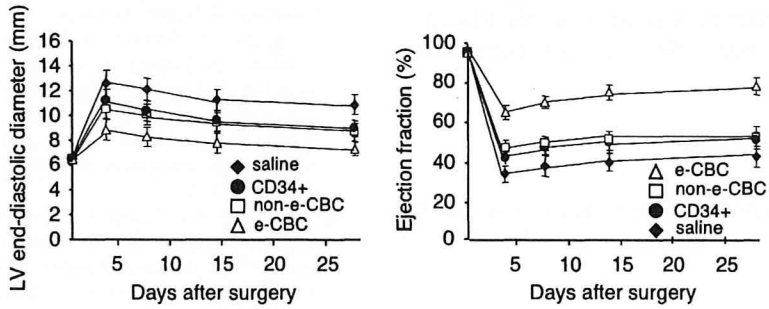

Fig. 4. e-CBCs transplantation improved cardiac function. LV diameter (LV end-diastolic diameter) and function (Ejection fraction) were assessed by echocardiography at 0, 3, 7, 14, and 28 days following myocardial infarction and injection of saline, e-CBCs, non-e-CBCs, and HSCs (CD34+). Note that in case of injection of e-CBCs, enlargement of LV diameter was reduced and LV function was significantly improved compared with injection of saline, non-e-CBCs, and HSCs. Each data point is the mean of five determinations; bars denote ±SD.

with the expression of Nkx2.5 and GATA-4 on CBMNCs (Fig. 2). In order to determine how e-CBCs differentiated into CMs, we tested a number of growth and survival factors and found that Akt activation seemed to play a role in the differentiation of CBMNCs into CMs (Supplemental data 1). Akt, a serine threonine kinase, transduces powerful survival signals in many systems [22,23]. Recently, it was reported that overexpression of Akt1 in MSCs increased the post-transplantation viability of these cells and enhanced their therapeutic efficiency [24]. In fact, intramyocardial injection of MSCs that had been transfected with a retroviral vector containing the Akt gene resulted in the

differentiation of MSCs into CMs and led to the prevention of ventricular remodeling and to the restoration of cardiac function after MI. In order to examine the survival signals in e-CBCs in each culture day as indicated, we checked the phosphorylation level of Akt (p-Akt) in e-CBCs on days 0, 3, and 7. Before extraction of cell lysate, e-CBCs were exposed to hypoxic condition for 24 h. The p-Akt level of e-CBCs on day 3 was 10-fold higher than that on day 7 and it was higher (1.7×) than that on day 0 before coculturing with BATDCs (Supplement data 1). The resistance of cell to apoptosis induced by hypoxic stimuli was proportional to the level of p-Akt in e-CBCs, i.e., it was higher on day 3 compared to day 0 and day 7. This anti-apoptotic effect might contribute to the high incidence of CMs derived from e-CBCs and to prevention of cardiac remodeling caused by conditions such as hypoxia, inflammation, and mechanical stress, and many endogenous factors such as angiotensin II, endothelin-1, and norepinephrine [25] in MI model.

We have as yet not clarified the precise mechanism whereby CB cells expressed high levels of p-Akt in hypoxic conditions after short-term coculturing with BATDCs. BATDCs were derived from adipose tissue, which possessed many beneficial factors, such as vascular endothelial growth factor (VEGF), hepatocyte growth factor (HGF), angiopoietin-1, and so on [16]. Therefore, these factors might support the high level of p-Akt in e-CBCs. Identification of such factors may enable effective myocardial regeneration. Use of CBCs together with such factors for protection against cell apoptosis may enable the application of the strategy described here to the clinic for managing patients of ischemic disease.

Acknowledgments

We thank Miss M. Sato for technical support. This study was supported in part by a grant from the Ministry of Education, Culture, Sports, Science, and Technology of Japan.

Appendix A. Supplementary data

Supplementary data associated with this article can be found, in the online version, at doi:10.1016/j.bbrc.2006.12.017.

References

[1] S. Makino, K. Fukuda, S. Miyoshi, F. Konishi, H. Kodama, J. Pan, M. Sano, T. Takahashi, S. Hori, H. Abe, J. Hata, A. Umezawa, S. Ogawa, Cardiomyocytes can be generated from marrow stromal cells in vitro, J. Clin. Invest. 103 (1999) 697–705.

[2] C. Toma, M.F. Pittenger, K.S. Cahill, B.J. Byrne, P.D. Kesseler, Human mesencymal stem cells differentiate to a cardiomyocyte phenotype in adult murine heart, Circulation 105 (2002) 93–98.

[3] S. Tomita, R.K. Li, R.D. Weise, D.A. Mickle, E.J. Kim, T. Sakai, Z.Q. Jia, Autologous transplantation of bone marrow cells improves damaged heart function, Circulation 100 (1999) 247–256.

[4] I. Kehat, D. Kenyagin-Karsenti, M. Snir, M. Segev, M. Amit, A. Gepstein, E. Livne, O. Binah, J. Itskovitz-Eldor, L. Gepstein, Human embryonic stem cells can differentiate into myocytes with structural and functional properties of cardiomyocytes, J. Clin. Invest. 108 (2001) 407–414.

[5] I. Kehat, A. Gepstein, A. Spira, J. Itskovitz-Eldor, L. Gepstein, High-resolution electrophysiological assessment of human embryonic stem cell-derived cardiomyocytes: a novel in vitro model for the study of conduction, Circ. Res. 91 (2002) 659–661.

[6] A.P. Beltrami, L. Barlucchi, D. Torella, M. Baker, F. Limana, S. Chimenti, H. Kasahara, M. Rota, E. Musso, K. Urbanek, A. Leri, J. Kajstura, B. Nadal-Ginard, P. Anversa, Adult cardiac stem cells are multipotent and support myocardial regeneration, Cell 114 (2003) 763–776.

[7] H. Oh, S.B. Bradfute, T.D. Gallardo, T. Nakamura, V. Gaussin, Y. Mishina, J. Pocius, L.H. Michael, R.R. Behringer, D.J. Garry, M.L. Entman, M.D. Schneider, Cardiac progenitor cells from adult myocardium: homing, differentiation, and fusion after infarction, Proc. Natl. Acad. Sci. USA 100 (2003) 12313–12318.

[8] H. Mayani, P.M. Lansdorp, Biology of human umbilical cord blood derived hematopoietic stem/progenitor cells, Stem Cells 16 (1998) 153–165.

[9] A. Erices, P. Congnet, J.J. Minguell, Mesenchymal progenitor cells in human umbilical cord blood, Br. J. Haemotol. 109 (2000) 235–242.

[10] S.J. Szilvassy, T.E. Meyerrose, P.L. Ragland, B. Grimes, Differentioal homing and engraftment properties of hematopoietic progenitor cells from murine bone marrow, mobilized peripheral blood, and fetal liver, Blood 98 (2001) 2108–2115.

[11] H. Vaziri, W. Dragowska, R.C. Allsopp, T.E. Thomas, C.B. Harley, P.M. Lansdorp, Evidence for a mitotic clock in human hematopoietic stem cells: loss of telomeric DNA with age, Proc. Natl. Acad. Sci. USA 91 (1994) 9857–9860.

[12] E.D. Zanjani, J.L. Ascensao, M. Tavassoli, Liver derived feta hematopoietic stem cells selectively and preferentially home to the fetal bone marrow, Blood 81 (1993) 399–404.

[13] N. Ma, Y. Ladilov, J.M. Moebius, L. Ong, C. Piechaczek, A. David, A. Kaminski, Y.H. Choi, W. Li, D. Egger, C. Stamm, G. Steinhoff, Intramyocardial delivery of human CD133+ cells in a SCID mouse cryoinjury model: bone marrow vs. cord blood-derived cells, Cardiovasc. Res. 71 (2006) 158–169.

[14] Y. Hirata, M. Sata, N. Motomura, M. Takanashi, Y. Suematsu, M. Ono, S. Takamoto, Human umbilical cord blood cells improve cardiac function after myocardial infarction, Biochem. Biophys. Res. Commun. 327 (2005) 609–614.

[15] G. Kogler, S. Sensken, J.A. Airey, T. Trapp, M. Muschen, N. Feldhahn, S. Liedtke, R.V. Sorg, J. Fischer, C. Rosenbaum, S. Greschat, A. Knipper, J. Bender, O. Degistirici, J. Gao, A.I. Caplan, E.J. Colletti, G. Almeida-Porada, H.W. Muller, E. Zanjani, P. Wernet, A new human somatic stem cell from placental cord blood with intrinsic pluripotent differentiation potential, J. Exp. Med. 200 (2004) 123–135.

[16] Y. Yamada, X.D. Wang, S.-I. Yokoyama, N. Fukuda, N. Takakura, Cardiac Progenitor cells in brown adipose tissue repaired damaged myocardium, Biochem. Biophys. Res.Commun. 343 (2006) 662–670.

[17] Y. Yamada, N. Takakura, H. Yasue, H. Ogawa, H. Fujisawa, T. Suda, Exogenous clustered neuropilin 1 enhances vasculogenesis and angiogenesis, Blood 97 (2001) 1671–1678.

[18] F. Ishikawa, H. Shimazu, L.D. Shultz, M. Fukata, R. Nakamura, B. Lyons, K. Shimoda, S. Shimoda, T. Kanemaru, K. Nakamura, H. Ito, Y. Kaji, A.C. Perry, M. Harada, Purified human hematopoietic stem cells contribute to the generation of cardiomyocytes through cell fusion, FASEB J. 20 (2006) 950–952.

[19] M. Alvarez-Dolado, R. Pardal, J.M. Garcia-Verdugo, J.R. Fike, H.O. Lee, K. Pfeffer, C. Lois, S.J. Morrison, A. Alvarez-Buylla, Fusion of bone-marrow-derived cells with Purkinje neurons, cardiomyocytes and hepatocytes, Nature 425 (2003) 968–973.

[20] D. Orlic, J. Kajstura, S. Chimenti, I. Jakoniuk, S.M. Anderson, B. Li, J. Pickel, R. Mckay, B. Nadal-Ginard, D.M. Bodine, A. Leri, P.

Anversa, Bone marrow cells regenerate infarcted myocardium, Nature 410 (2001) 701–705.
[21] H. Kawada, J. Fujita, K. Kinjo, Y. Matsuzaki, M. Tsuma, H. Miyatake, Y. Muguruma, K. Tsuboi, Y. Itabashi, Y. Ikeda, S. Ogawa, H. Okano, T. Hotta, K. Ando, K. Fukuda, Nonhematopoietic mesenchymal stem cells can be mobilized and differentiate into cardiomyocytes after myocardial infarction, Blood 104 (2004) 3581–3587.
[22] T.F. Franke, D.R. Kaplan, L.C. Cantley, PI3K: downstream AKTion blocks apoptosis, Cell 88 (1997) 435–437.
[23] S.R. Datta, A. Brunet, M.E. Greenberg, Cellular survival: a play in three Akts, Genes Dev. 13 (1999) 2905–2927.
[24] A.A. Mangi, N. Noiseux, D. Kong, H. He, M. Rezvani, J.S. Ingwall, V.J. Dzau, Mesenchymal stem cells modified with Akt prevent remodeling and restore performance of infarcted hearts, Nat. Med. 9 (2003) 1195–1201.
[25] H. Takano, Y. Qin, H. Hasegawa, K. Ueda, Y. Niitsuma, M. Ohtsuka, I. Komuro, Effects of G-CSF on left ventricular remodeling and heart failure after acute myocardial infarction, J. Mol. Med. 84 (2006) 185–193.

Neuroscience 144 (2007) 1425–1435

EXPRESSION OF ANGIOGENIC AND NEUROTROPHIC FACTORS IN THE PROGENITOR CELL NICHE OF ADULT MONKEY SUBVENTRICULAR ZONE

A. B. TONCHEV,[a,b] T. YAMASHIMA,[a*] J. GUO,[a] G. N. CHALDAKOV[b] AND N. TAKAKURA[c1]

[a]*Department of Restorative Neurosurgery, Division of Neuroscience, Kanazawa University Graduate School of Medical Science, Takaramachi 13-1, Kanazawa, 920-8641 Japan*

[b]*Division of Cell Biology, Department of Forensic Medicine, Medical University of Varna, Varna, Bulgaria*

[c]*Department of Stem Cell Biology, Cancer Research Institute, Kanazawa University, Kanazawa, Japan*

Abstract—The subventricular zone along the anterior horn (SVZa) of the cerebral lateral ventricle of adult mammals contains multipotent progenitor cells, which supposedly exist in an angiogenic niche. Numerous signals are known to modulate the precursor cell proliferation, migration or differentiation, in rodent models. In contrast, the data on signals regulating the primate SVZa precursors *in vivo* are scarce. We analyzed the expression at protein level of a panel of angiogenic and/or neurotrophic factors and their receptors in SVZa of adult macaque monkeys, under normal condition or after transient global ischemia which enhances endogenous progenitor cell proliferation. We found that fms-like tyrosine kinase 1 (Flt1), a receptor for vascular endothelial cell growth factor, was expressed by over 30% of the proliferating progenitors, and the number of Flt1-positive precursors was significantly increased by the ischemic insult. Smaller fractions of mitotic progenitors were positive for the neurotrophin receptor tropomyosin-related kinase (Trk) B or the hematopoietic receptor Kit, while immature neurons expressed Flt1 and the neurotrophin receptor TrkA. Further, SVZa astroglia, ependymal cells and blood vessels were positive for distinctive sets of ligands/receptors, which we characterized. The presented data provide a molecular phenotypic analysis of cell types comprising adult monkey SVZa, and suggest that a complex network of angiogenic/neurotrophic signals operating in an autocrine or paracrine manner may regulate SVZa neurogenesis in the adult primate brain.

Key words: cerebral ischemia, primate, neurogenesis, Flt1, TrkB, Kit.

The subventricular zone of the anterior horn (SVZa) of the cerebral lateral ventricle in adult mammals harbors neural progenitor cells which are capable of glial and neuronal production. These cells have been studied extensively in non-primate mammalian species, and a number of molecular signals that affect their proliferation and differentiation have been identified (reviewed by Okano, 2002; Lledo et al., 2006). Cerebral injuries such as ischemia up-regulate SVZa progenitors in both focal (Jin et al., 2001; Zhang et al., 2001; Arvidsson et al., 2002; Parent et al., 2002) and global (Iwai et al., 2003) rodent ischemic models. The ischemia-triggered activation of endogenous precursors can be further enhanced by external application of trophic factors (reviewed by Zhang et al., 2005; Lichtenwalner and Parent, 2006). Existence of progenitor cells was described also in SVZa of normal adult primates, including both humans (Pincus et al., 1998; Sanai et al., 2004) and monkeys (Kornack and Rakic, 2001; Pencea et al., 2001a). Recently, we reported evidence that, similarly to the rodent brain, ischemia was capable of increasing the proliferation of SVZa precursors in a monkey model of transient global cerebral ischemia (Tonchev et al., 2005). Whether these similar responses between rodents and monkeys are mediated by identical or distinct molecular signals is currently unknown as the knowledge on the molecular regulation of primate SVZa progenitors is limited.

Recent evidence indicates that neural and vascular cells not only reciprocally affect their own growth by paracrine mechanisms (reviewed by Emanueli et al., 2003), but also use common signals (reviewed by Carmeliet, 2003). For example, neurotrophins such as nerve growth factor (NGF) and brain-derived neurotrophic factor (BDNF) promote angiogenesis (Calza et al., 2001; Kim et al., 2004). Reciprocally, vascular signaling affects neuronal precursor cells (Leventhal et al., 1999; Palmer et al., 2000; Palmer, 2002; Yamashima et al., 2004). In addition to its well-known role in angiogenesis, vascular endothelial growth factor (VEGF) promotes neurogenesis and neuroprotection by mediating both proliferation (Jin et al., 2002a) and chemoattraction (Zhang et al., 2003) of adult brain progenitors, under normal or ischemic (Sun et al., 2003) conditions. Importantly, a link between angiogenic and neurotrophic factors in regulating adult neurogenesis was established, by showing that endothelial cell-derived VEGF enhances neurogenesis in a BDNF-dependent manner (Louissaint et al., 2002).

In the present study, we investigated the expression at protein level of angiogenic and/or neurotrophic factors and their receptors in the progenitor cell niche of adult monkey

[1] Present address: Department of Signal Transduction, Research Institute for Microbial Diseases, Osaka University, Osaka, Japan.

*Corresponding author. Tel: +81-76-265-2381; fax: +81-76-231-1718.
E-mail address: yamashim@med.kanazawa-u.ac.jp (T. Yamashima).

Abbreviations: ac, anterior commissure; Ang, angiopoietin; BDNF, brain-derived neurotrophic factor; BrdU, bromodeoxyuridine; Flk, fetal liver kinase; Flt, fms-like tyrosine kinase; GDNF, glial cell line-derived neurotrophic factor; GFRα1, glial cell line-derived neurotrophic factor family receptor α1; NGF, nerve growth factor; Nrp, neuropilin; NT3, neurotrophin-3; PI, propidium iodide; SCF, stem cell factor; SVZa, anterior subventricular zone; Tie, tyrosine kinase with immunoglobulin-like and epidermal growth factor-like domains; TRITC, tetramethylrhodamine isothiocyanate; Trk, tropomyosin-related kinase; VEGF, vascular endothelial growth factor; vWF, von Willebrand factor.

0306-4522/07$30.00+0.00
doi:10.1016/j.neuroscience.2006.10.052

SVZa. We employed a primate model that has previously demonstrated an increased proliferation of SVZa precursors after ischemia (Tonchev et al., 2005). Our target was to determine the receptor(s) expressed by actively proliferating precursors as well as by other cellular phenotypes comprising SVZa, and thus to provide structural evidence for putative ligand/receptor interactions in adult monkey progenitor cell niche. Such evidence may be helpful in designing future studies devoted on establishing the precise involvement of each of the studied factors in the regulation of primate progenitor cells.

EXPERIMENTAL PROCEDURES

Animal procedures

Animal experiments were performed under strict adherence to the guidelines of the Animal Care and Ethics Committee of Kanazawa University, and the NIH Guide for the Care and Use of Laboratory Animals. All efforts were made to minimize the number of animals used and to reduce animal suffering throughout the experiments. The subjects of investigation were adult Japanese monkeys (*Macaca fuscata*), bred in air-conditioned cages, and allowed free daily access to food and water. A model of transient global cerebral ischemia was performed as previously described (Yamashima et al., 1998; Tonchev et al., 2005). Briefly, the sternum was resected under general anesthesia with artificial ventilation, and the innominate and left subclavian arteries were transiently ligated for 20 min. The effectiveness of clipping was demonstrated by an almost complete absence (0.5±1.0 ml/100 g brain/min) of cerebral blood flow as monitored by laser Doppler (Vasamedics, St. Paul, MN, USA). Ischemia was performed on six monkeys, while two monkeys underwent sham surgery (executed by opening the chest without vessel clipping). All monkeys received five daily injections of 100 mg/kg i.v. of bromodeoxyuridine (BrdU) (Sigma-Aldrich Japan K.K., Tokyo, Japan), performed on days 5–9 after surgery. Respective animals were then killed on day 9 (n=2), day 23 (n=2) and day 44 (n=2) and after ischemia or on day 9 (n=2) after the sham operation (Tonchev et al., 2005).

Histological processing

The monkeys were killed by lethal doses of sodium pentobarbital and intracardially perfused with ice-cold saline containing heparin followed by ice-cold solution of 4% paraformaldehyde. Upon removal of brain, tissue blocks corresponding to anterior commissure (ac) +7 mm anteriorly until ac +1 mm posteriorly were resected and submerged in 30% sucrose solution until they sank to the bottom. The tissues were then frozen in O.C.T. medium (Tissue-Tek, Sakura Finetech Co., Tokyo, Japan), and serially cut into 40-μm thick coronal sections. All stainings were performed on free-floating sections. Upon equilibrating sections in Tris-buffered saline containing 0.1% Triton X-100 (TBS-T) and appropriate blocking sera, the primary antibodies were applied (Table 1) for 48 h at 4 °C. We tested whether the use of the detergent Triton X-100 may prevent the successful immunostaining of membranous antigens such as the receptors of signaling molecules targeted in our study; in pilot experiments we used concentrations ranging from 0.01% to 0.1% Triton as well as no Triton in the buffer. As we did not observe differences among these formulations in respect to the quality of staining, we used 0.1% Triton because we thought it would provide a better reagent penetration in the 40-μm thick sections. VEGF was investigated concomitantly with its two principal receptors acting in the nervous system: the receptor tyrosine kinases fms-like tyrosine kinase (Flt) 1 and fetal liver kinase (Flk) 1, and the co-receptor Neuropilin 1 (Nrp1) (Fer-

Table 1. List of primary antibodies against signaling molecules and their receptors used in the study

Antibody against	Epitope	Species	Dilution	Reference	Vendor, cat. #
VEGF	N-terminus of human VEGF-A	Goat	1:200	Ruef et al., 1997	Santa Cruz Biotechnology (Santa Cruz, CA, USA); #sc-152
Flt1	Amino acids 23–247 of human Flt1	Rabbit	1:100	Tissot van Patot et al., 2004	Santa Cruz; #sc-9029
Flk1	Amino acids 1158–1345 of mouse Flk1	Rabbit	1:50	Ruef et al., 1997	Santa Cruz; #sc-504
Nrp1	Amino acids 570–855 of human Nrp1	Rabbit	1:200	Parikh et al., 2004	Santa Cruz; #sc-5541
Kit tyrosine kinase receptor	Amino acids 961–976 of human Kit	Rabbit	1:50	Gougeon and Busso, 2000	Calbiochem (LA Jolla, CA, USA); #PC34
Ang1	N-terminus of human Ang1	Goat	1:50	Otani et al., 1999	Santa Cruz; #sc-6319
Ang2	N-terminus of human Ang2	Goat	1:50	Otani et al., 1999	Santa Cruz; #sc-7016
Tie2	C-terminus of mouse Tie2	Rabbit	1:100	Otani et al., 1999	Santa Cruz; #sc-324
Tie1	C-terminus of human Tie1	Rabbit	1:100	Uchida et al., 2000	Santa Cruz; #sc-342
NGF	Amino acids 1–20 of human NGF	Rabbit	1:200	Quartu et al., 1999	Santa Cruz; #sc-548
BDNF	Amino acids 1–20 of human BDNF	Rabbit	1:200	Hayashi et al., 2001	Santa Cruz; #sc-546
NT3	Amino acids 139–158 of human NT3	Goat	1:200	Quartu et al., 1999	Santa Cruz; #sc-13380
TrkA	Amino acids 763–777 of human TrkA	Rabbit	1:200	Quartu et al., 2003	Santa Cruz; #sc-118
TrkB	Amino acids 794–808 of mouse TrkB	Rabbit	1:200	Hayashi et al., 2000	Santa Cruz; #sc-12
TrkC	Amino acids 798–812 of porcine TrkC	Rabbit	1:200	Sandell et al., 1998	Santa Cruz; #sc-117
Pan-neurotrophin receptor of 75 kD (p75NTR)	Amino acids 1–160 of human p75	Mouse	1:50	Sandell et al., 1998	Dako (Kyoto, Japan); #M3507
GDNF	Recombinant human GDNF	Goat	1:100	Serra et al., 2002	R&D Systems (Minneapolis, MN, USA); #AF-212-NA
GFRα1	Amino acids 368–437 of human GFRα1	Rabbit	1:200	Serra et al., 2005	Santa Cruz; #sc-10716
Ret tyrosine kinase receptor	C-terminus of human Ret	Goat	1:200	Walker et al., 1998	Santa Cruz; #sc-1290

References describe previous use of each antibody in primate neural or non-neural tissues.

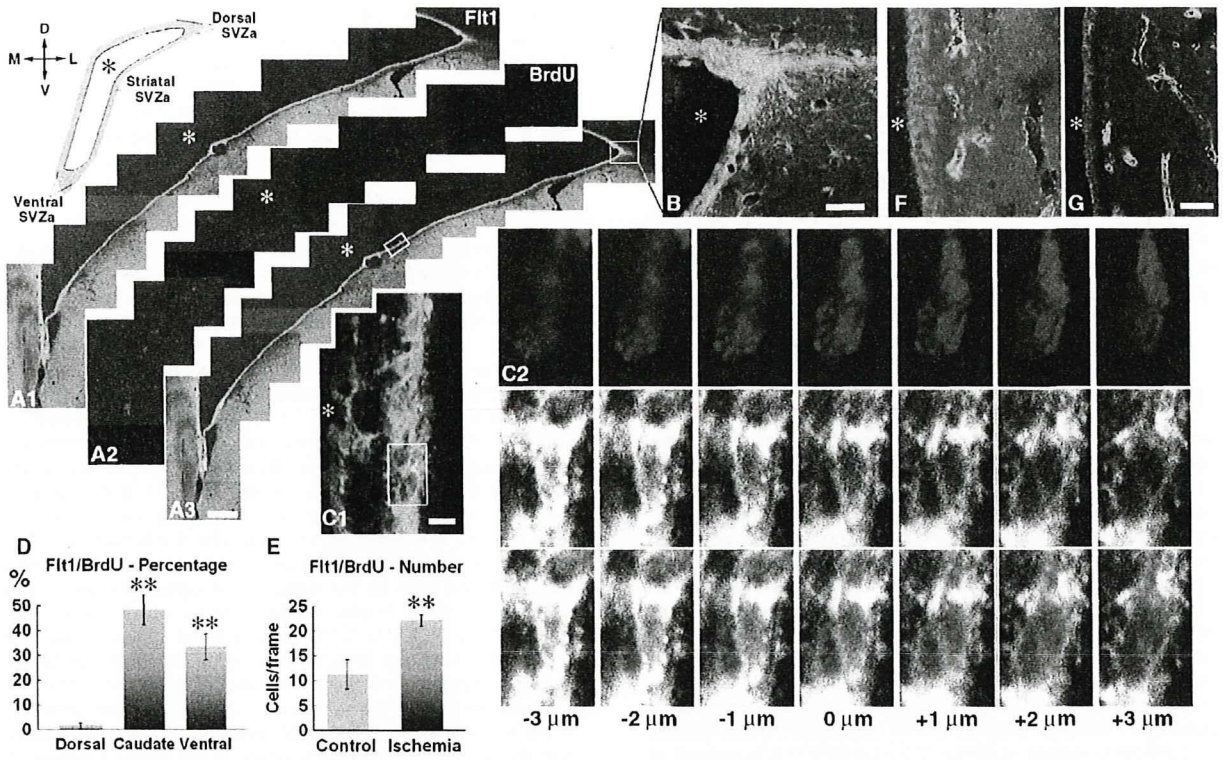

Fig. 1. Expression of Flt1 in SVZa. (A) Photomontages of low magnification micrographs showing the distribution of Flt1 (A1) and BrdU (A2) positive signals in SVZa, and overlay (A3). The positions of the SVZa aspects are depicted on the schematic map (upper left; D, dorsal; V, ventral; M, medial; L, lateral). Note that both Flt1$^+$ and BrdU$^+$ cells are preferentially localized along the lumen of the ventricle. (B) Higher power view of Flt1 (green) and BrdU (red) double-staining on day 9 in dorsal SVZa. Note lack of double-stained cells. (C) Flt1 and BrdU (red) double-staining in striatal SVZa on day 9. (C1) A Flt1$^+$/BrdU$^+$ cell cluster is focused (frame). (C2) The cluster is presented as consecutive 1-μm optical sections in the *z* axis to demonstrate the co-localization of the signals (the Flt1 signal is shown in white to achieve a better contrast). (F) Percentage of BrdU$^+$ cells co-labeled for Flt1 in various SVZa aspects. * $P<0.01$ versus dorsal SVZa. (G) Absolute number of BrdU$^+$ cells co-labeled for Flt1 in control and postischemic SVZa (dorsal, striatal, ventral). ** $P<0.01$ versus control. Expression of Flk1 in SVZa, and control stainings. The top panel shows Flk1 immunoreactivity in a subependymal blood vessel (bv). Positive cells outside the vascular wall are absent. The bottom panels depict negative control stainings by omitting primary antibody. Similar results were obtained by using pre-adsorption with specific blocking peptides. Scale bars=400 μm (A); 40 μm (B); 10 μm (C); 50 μm (D, E). Asterisk, lateral ventricle.

rara et al., 2003). Kit (CD117), the receptor for stem cell factor (SCF), might be implicated in angiogenesis by its expression on hematopoietic and circulating endothelial progenitor cells (Li et al., 2003). SCF stimulates endogenous neural progenitor cells after cerebral ischemia in rodents (Jin et al., 2002b; Kawada et al., 2006). We investigated NGF, BDNF and their cognate receptors, because both NGF (Calza et al., 2003) and BDNF *in vivo* affect SVZa progenitors in rodents (Pencea et al., 2001b; Benraiss et al., 2001) and monkeys (Bedard et al., 2006). We particularly noticed the relation of neurotrophin and VEGF immunoreactivities (Calza et al., 2001; Louissaint et al., 2002). Other neurotrophic factors, neurotrophin-3 (NT3) (Ghosh and Greenberg, 1995) and glial cell line-derived neurotrophic factor (GDNF) (Chen et al., 2005), have also been reported to affect brain progenitor cells in rodent models, and GDNF was implicated in postischemic precursor proliferation (Dempsey et al., 2003), but their involvement in the primate progenitor cell niche is unclear; thus they were investigated.

In addition to antibodies directed against signaling molecules or their receptors, we used the following antibodies against phenotypic markers: mouse anti-BrdU (1:100, Becton Dickinson, San Jose, CA, USA), rat anti-BrdU (1:100, Harlan Sera-Laboratory, Loughborough, UK), mouse anti-Nestin (Chemicon, Temecula, CA, USA), rabbit or mouse anti-β-tubulin class III (1:400, Covance, Richmond, CA, USA), rabbit anti-glial fibrillary acidic protein (GFAP) (1:400, Sigma; or DAKO Japan K.K., Kyoto, Japan), mouse anti-S100β (1:500, Sigma), mouse anti-CD31 (1:50, DAKO), and rabbit anti-von Willebrand factor (vWF) (1:200; DAKO). To reveal BrdU incorporated into DNA of cells, DNA was denatured by sequentially incubating sections in formamide and HCl as described (Tonchev et al., 2005), followed by application of primary antibodies. The primary antibodies were revealed by appropriate secondary antibodies conjugated to AlexaFluor 488, 546, or 633 (Molecular Probes, Eugene, OR, USA), tetramethylrhodamine isothiocyanate (TRITC; Jackson Immunoresearch, West Grove, PA, USA), or to biotin for immunoperoxidase labeling (1:30–1:100; Vector ABC kit, Vector Laboratories, Burlingame, CA, USA). For double- and triple-staining, primary antibodies were from different species, and were applied sequentially to minimize the probability for cross-reactivity. For Flt1/Kit double-staining using two rabbit antibodies, just before the second primary, the first primary was masked by a large excess of unconjugated secondary antibody (anti-rabbit IgG; Vector) (Lewis Carl et al., 1993; Muzio et al., 2002).

Antibody specificity

All of the antibodies used in the present study have been previously characterized on primate (monkey or human) tissues (see references list in Table 1). The antibodies directed against neu-

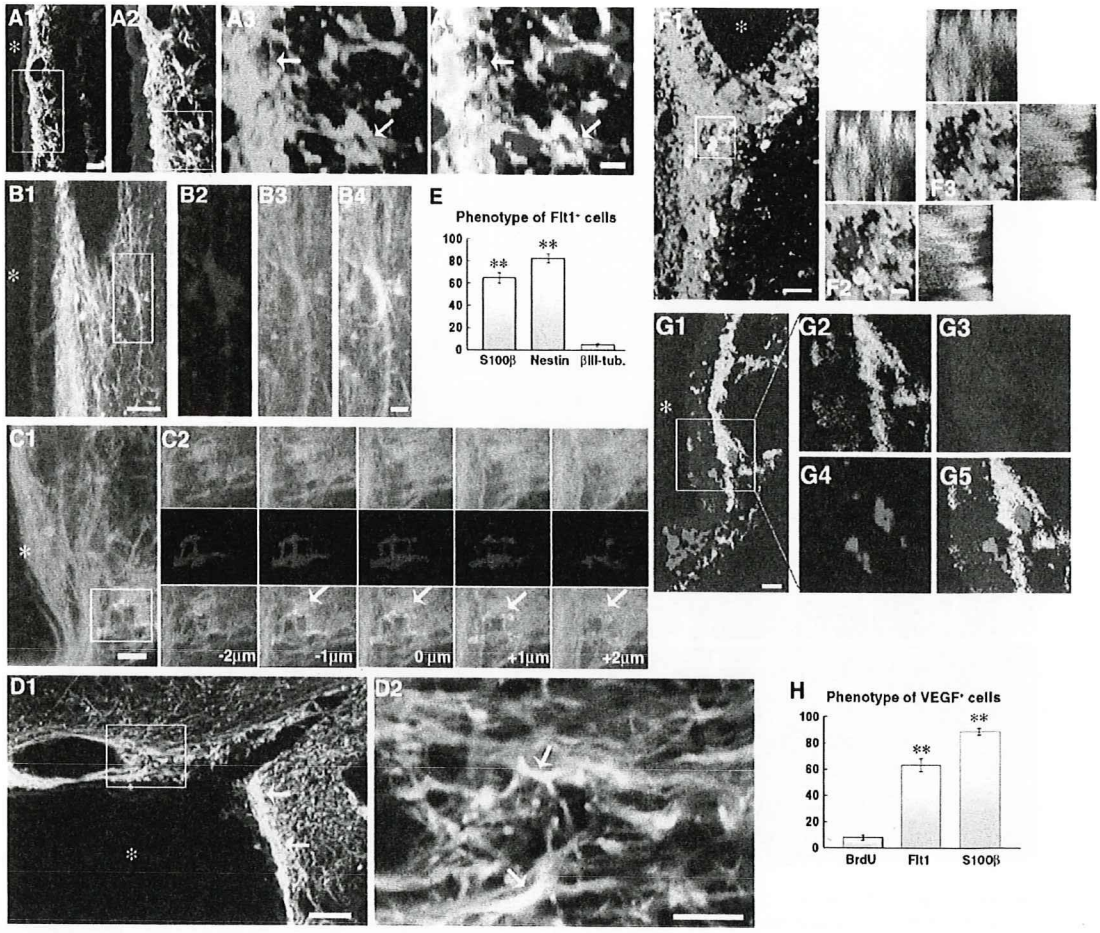

Fig. 2. Phenotype of Flt1$^+$ and VEGF$^+$ cells in SVZa. (A) Double-staining for Flt1 (green) and S100β (red) on day 9. The boxed region in A1 is magnified in A2, and the boxed region on A2 is magnified with channel separation in A3. Flt1$^+$/S100β^+ cells appear yellow (arrows). (B) Double-staining for Flt1 (green) and nestin (red) on day 9. The boxed region in B1 is magnified with channel separation in B2–B4. (C) Double-staining for Flt1 (green) and βIII-tubulin (red) on day 44. The cluster depicted by a box (C1) is shown as consecutive optical sections in the *z* axis (C2) to confirming the co-localization of the signals (a 3D reconstruction of this cluster is presented in Supplementary movie 2). (D) Double-labeling for Flt1 (green) and VEGF (red) on day 9 in dorsal SVZa. Boxed area in D1 is magnified in D2. Flt1$^+$/VEGF$^+$ cells appear in yellow (the arrow shows an example) while some Flt1$^-$/VEGF$^+$ cells appear in red. (E) Percentages of Flt1$^+$ cells co-labeled for cell markers. ** $P<0.01$ versus βIII-tubulin. (F) Double-staining for VEGF (green) and BrdU (red) on day 23. While many BrdU cells are negative for VEGF, a double-labeled cluster (boxed area in F1) is presented with orthogonal projections in the *x* and *y* axes in F2 and F3. (G) Triple-labeling for VEGF, S100β and βIII-tubulin on day 9 in striatal SVZa. G1 depicts low magnification overlay view of the three channels, with the boxed area presented with channel separation; G2 (VEGF), G3 (S100β), G4 (βIII-tubulin), G5 (overlay). Note that VEGF$^+$ and βIII-tubulin$^+$ cells are spatially adjacent but distinct. (H) Percentages of VEGF$^+$ cells co-labeled for cell markers. ** $P<0.01$ versus BrdU. Scale bars=50 μm (D1); 20 μm (A1, F1); 10 μm (B1, C1, G1); 5 μm (A4, B4, D2, F2). Asterisk, lateral ventricle.

rotrophins (NGF, BDNF, NT3, GDNF) or their receptors have been characterized on primate brains by both immunohistochemistry and Western blot (Quartu et al., 1999, 2003; Hayashi et al., 2000, 2001; Sandell et al., 1998; Serra et al., 2002, 2005; Walker et al., 1998). Staining monkey brain regions outside of SVZa with these antibodies yielded a pattern similar to the above-cited studies (data not shown). The antibodies directed against angiogenic factors or their receptors have been characterized in non-neural primate tissues (Ruef et al., 1997; Otani et al., 1999; Gougeon and Busso, 2000; Tissot van Patot et al., 2004; Parikh et al., 2004). To determine the specificity of the primary antibodies, these were pre-absorbed with 10-fold excess of blocking peptides, where such peptides were available: anti-VEGF, anti-Nrp1, anti-NGF, anti-BDNF, anti-NT3, anti-tropomyosin-related kinase (Trk) A, anti-TrkB, anti-TrkC, anti-angiopoietin (Ang) 1, anti-Ang2, anti-tyrosine kinase with immunoglobulin-like and epidermal growth factor-like domains (Tie) 1, anti-Tie2, and anti-Ret. Negative control experiments were also performed by omitting the primary antibody. All these control stainings revealed no positivity (Supplementary Fig. 1).

Image analysis

Double- and triple-labeling to determine the expression of signaling molecules or their receptors by BrdU-labeled cells or cells labeled for particular phenotypic markers was evaluated using confocal laser scanning microscopy (LSM 510, Carl Zeiss, Tokyo, Japan). Alexa Fluor 488 was appointed in the green channel, TRITC or Alexa Fluor 546, in the red channel, and Alexa Flour 633, in the blue channel. We undertook specific steps to avoid "leakage" ("bleed-through") of signal among the channels, e.g. to visualize an intense green signal in the red

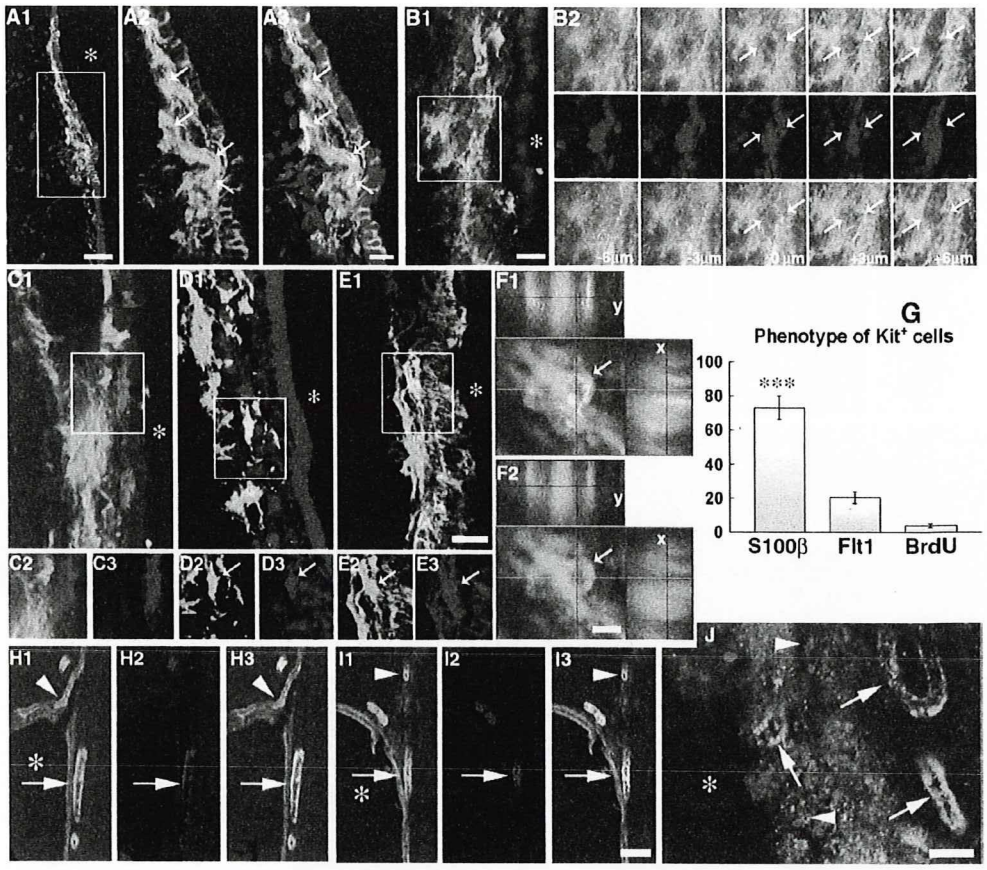

Fig. 3. Phenotype of Kit$^+$ cells in SVZa. (A) Kit immunoreactivity (green) in striatal SVZa, counterstained by PI (red). The boxed region in A1 is magnified with channel separation in A2 and A3. Note the subependymal localization of the Kit$^+$ cells (arrows). (B) Higher magnification view of Kit immunoreactivity (green) in striatal SVZa, counterstained by PI (red). The boxed region in B1 is presented as consecutive 1-μm optical sections in the *z* axis. Note a PI$^-$ cluster (arrows) does not express Kit, which is confirmed by a 3D reconstruction (Supplementary movie 2). (C) Double-labeling for Kit (green) and βIII-tubulin (red) on day 23. The boxed region in C1 is magnified with channel separation in C2 and C3. (D) Double-labeling for Kit (green) and S100β (red) on day 9. The boxed region in D1 is magnified with channel separation in D2 and D3. A double-positive cell is depicted by arrow. (E) Double-labeling for Kit (green) and Flt1 (red) on day 9. The boxed region in E1 is magnified with channel separation in E2 and E3. A double-positive cell is depicted by arrow. (F) Double-labeling for Kit (green) and BrdU (red) on day 9. A double-positive cell Kit/BrdU cell (arrow) is presented in a merged image (F1) or Kit channel only (F2) with orthogonal projections in the *x* and *y* axes. (G) Percentages of Kit$^-$ cells co-labeled for cell markers. *** $P<0.001$ versus Flt1/BrdU. (H) Double-staining for CD31 (H1) and Ang1 (H2), and overlay (H3) in SVZa, day 9. (I) Double-staining for CD31 (I1) and Tie2 (I2), and overlay (I3) in SVZa, day 9. CD31$^+$/Ang1$^+$ and CD31$^-$/Tie2$^+$ vessels are depicted by arrows. Not all blood vessels are positive for Ang1 or Tie2 (CD31$^+$/Ang1$^-$ and CD31$^+$/Tie2$^-$ vessels are depicted by arrowheads). (J) Double-staining for Tie1 (green) and BrdU (red) in SVZa, day 9. Tie1$^+$ blood vessels (arrows) and BrdU$^+$ cells (arrowheads) do not co-label. Asterisk, lateral ventricle. Scale bars=50 μm (A, H, I), 20 μm (B–E, J), 5 μm (F2). Asterisk, lateral ventricle.

channel. Thus, each fluorochrome was assigned to be scanned separately and sequentially to minimize the probability of signal transfer among channels. Z sectioning at 0.5–1 μm intervals was performed and optical stacks of at least 20 images were used for analysis. Digital three-dimensional reconstructions were created by the Zeiss LSM software version 2.3. Within each animal group, at least 150 cells positive for BrdU or a phenotypic marker were sampled for co-expression with respective transcription factors. The absolute numbers of transcription factor/BrdU double-positive cells were determined by multiplying the corresponding fractions with the total numbers of BrdU$^+$ cells evaluated on every 12th section stained by the peroxidase method within grids of 800 μm×100 μm placed in the dorsal, ventral, and striatal aspects of SVZa (see Fig. 1A) as previously described (Tonchev et al., 2005). Numbers and percentages were averaged to obtain a mean density value for each transcription factor/animal group.

Statistical analysis

For comparing percentages of cells expressing certain transcription factor, we applied nonparametric tests (Mann-Whitney *U* test and Kruskal-Wallis test) or one-way ANOVA followed by Tukey-Kramer's post hoc comparisons. Data were expressed as means±S.E.M. Differences were considered significant when $P<0.05$.

RESULTS

Flt1 was expressed by proliferating progenitors

Staining for Flt1 in monkey SVZa revealed an intense positive signal in the dorsal, striatal and ventral SVZa aspects (Fig. 1A), which showed increased numbers of

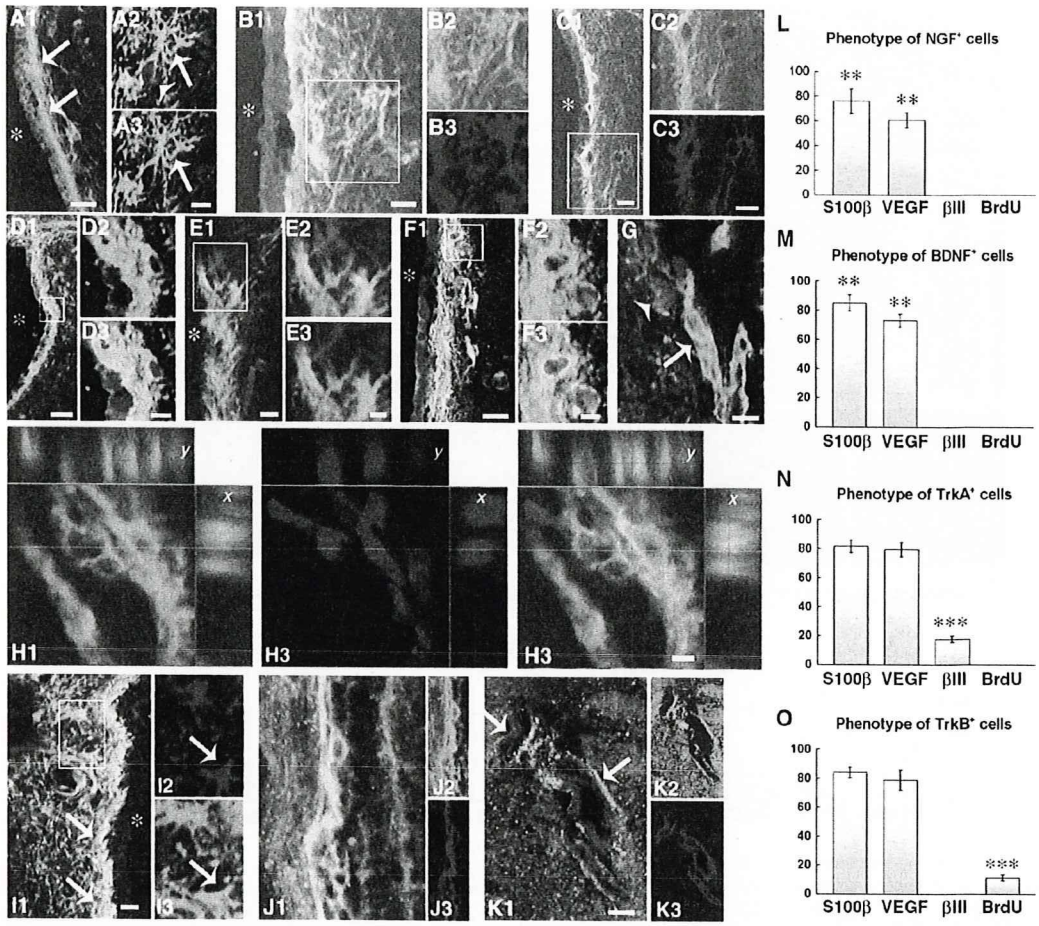

Fig. 4. NGF, BDNF, and their receptors in SVZa. (A) Single-labeling for NGF, day 9 (A1) demonstrating positive band of cells in SVZa (arrows), followed by double-labeling (A2, A3) for NGF (green; arrow) and BrdU (red; arrowhead) demonstrating lack of co-labeling. (B) Double-staining for NGF (green) and S100β (red), control. Double-positive cells appear in yellow. The boxed region in B1 is presented with channel separation in B2 and B3. (C) Double-labeling for NGF (green) and VEGF, day 9. Double-positive cells appear in yellow. The boxed region in C1 is magnified with channel separation in C2 and C3. (D) Double-staining for BDNF (green) and S100β (red), day 9. Double-positive cells appear in yellow. The boxed region in D1 is magnified with channel separation in D2 and D3. (E) Double-labeling for BDNF (green) and βIII-tubulin (red), day 9. The boxed region in E1 is magnified with channel separation in E2 and E3. Note the lack of co-labeling. (F) Double-staining for TrkB (green) and S100β (red), day 9. Double-positive cells appear in yellow. The boxed region in F1 is magnified with channel separation in F2 and F3. (G) Double-staining for TrkA (green; arrows) and BrdU (red; arrowhead), day 9. Note lack of co-labeling. (H) Double-staining for TrkB (H1), BrdU (H2), and overlay (H3), day 9. A double-positive cluster is depicted, with orthogonal projections in the *x* and *y* axes. (I) Double-staining for TrkB (green) and VEGF (red), day 9. Note extensive subependymal co-labeling (arrows). The boxed region in I1 is magnified in I2 and I3 depicting a double-labeled stellate cell (arrows). (J) Double-staining for TrkA (green), and βIII-tubulin (red) in striatal SVZa, day 9. The double-positive cells appear with a honeycomb pattern in yellow. The boxed region in J1 is magnified with channel separation in J2 and J3. (K) Double-staining for 75 kD pan-neurotrophin receptor (p75NTR) and vWF (K1), with channel separations in K2 and K3, day 23. (L–O) Percentages of NGF$^+$, BDNF$^+$, TrkA$^+$ and TrkB$^+$ cells, respectively, co-labeled for cell markers; ** $P<0.01$; *** $P<0.001$. Scale bars=50 μm (D1); 20 μm (A1, C, F1); 10 μm (A3, B1, D2, E1, G, I1, J, K); 5 μm (E3, F3, H3). Asterisk, lateral ventricle.

proliferating (BrdU$^+$) progenitors after ischemia (Tonchev et al., 2005). Extension of the Flt1 immunoreactivity in the rostral migratory stream toward the olfactory bulb was not observed (Fig. 1A3). Careful investigation for Flt1/BrdU co-labeling under high magnification revealed that in the dorsal SVZa double-stained cells were rare (Fig. 1B), while in the striatal (Fig. 1C) or ventral (Fig. 1D) SVZa such cells were frequently observed. The finding of Flt1/BrdU-labeled clusters (Fig. 1C) was paralleled by data showing formation of Flt1$^+$ clusters in stainings using the DNA-binding dye propidium iodide (PI) to label all nuclei. Significantly higher percentages of Flt1$^+$/BrdU$^+$ cells were identified in striatal or ventral SVZa as compared with its dorsal aspect (Fig. 1D). Further, ischemia increased the total number of Flt1$^+$/BrdU$^+$ cells in SVZa on day 9 as compared with controls (Fig. 1E). Flt1/BrdU co-expression at a long-term survival time points (day 23 or 44) was negligible (data not shown). In contrast to Flt1, Flk1 and the VEGF co-receptor Nrp1 were restricted to the vascular wall (Fig. 1F, G), in particular endothelial cells.

Most Flt1$^+$ cells co-labeled with S100β and nestin (Fig. 2A, B, E), with no statistically significant difference between control and ischemic monkeys. Co-staining of Flt1 with the neuronal marker βIII-tubulin was rare (Fig. 2C, E).

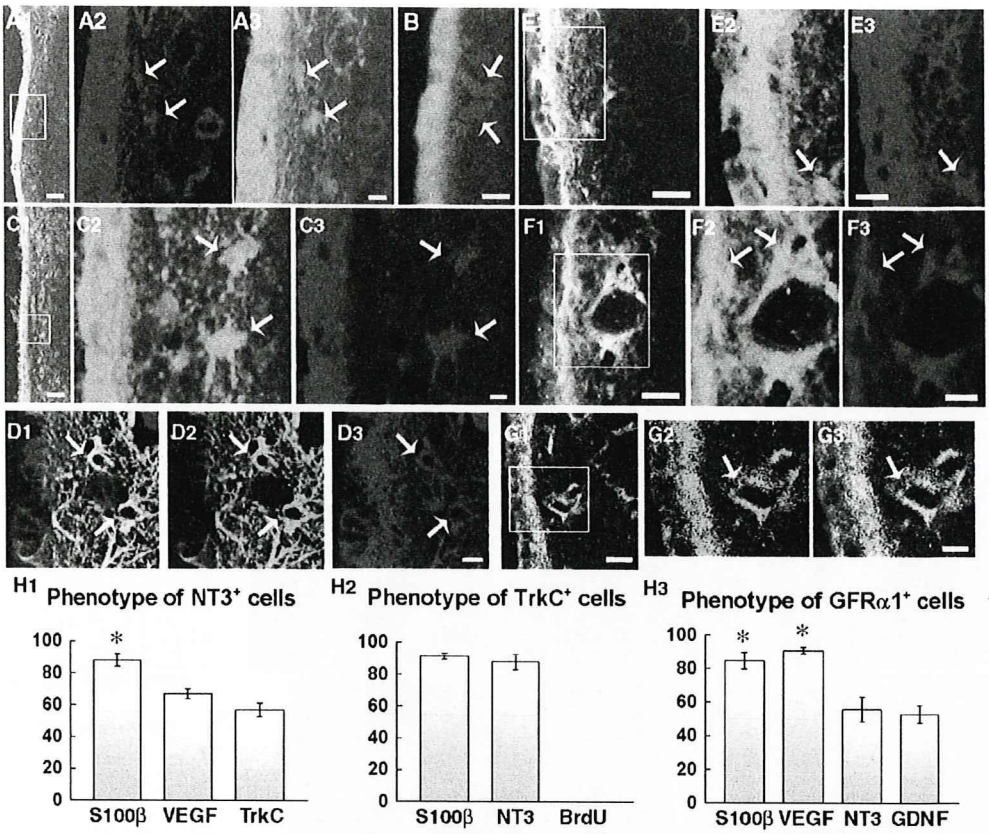

Fig. 5. NT3, GDNF, and their receptors in SVZa. (A) Double-staining for TrkC (green) and NT3 (red), day 9. The boxed zone (A1) is magnified in A2 and A3. In addition to the ependymal layer, some subependymal cells are double-labeled (arrows). (B) Double-staining for TrkC (green) and BrdU (red; arrows), day 9. Note lack of co-labeling. (C) Double-staining for S100β (green) and NT3 (red), day 9. Subependymal astrocytes cells are double-positive (arrows). The boxed region (C1) is magnified in C2 and C3. (D) Double-staining for VEGF (green, D2) and NT3 (red, D3), and overlay (D1), in control SVZa. Double-positive subependymal cell with stellate morphology are depicted by arrows. (E) Triple-labeling for GFRα1 (green), NT3 (red) and S100β (blue), day 9. The boxed region (E1) is magnified with channel separation in E2 and E3. A subependymal GFRα1$^+$ cell is co-stained for NT3 (arrow), while the strongly positive for S100β ependyma (appearing in pink in the overlay, A1) is co-labeled for NT3 but not for GFRα1. (F) Triple-labeling for GFRα1 (green), VEGF (red) and S100β (blue), day 9. The boxed region (F1) is magnified with channel separation in F2 and F3. The immunoreactivity of both GFRα1 and VEGF is largely subependymal and co-localizes on perivascular cells (arrows). (G) Double-staining for GFRα1 (green) and GDNF (red), day 9. The boxed zone (G1) is magnified in G2 and G3. A double-stained subependymal blood vessel is depicted by an arrow. (H) Percentages of NT3$^+$, TrkC$^+$ and GFRα1$^+$ cells, respectively, co-labeled for cell markers; * $P<0.05$. Scale bar=50 μm (A1, C1); 20 μm (E1, F1, G1); 10 μm (A3, B, C3, D3, E3, F3, G3). Asterisk, lateral ventricle.

Double-staining for Flt1 and VEGF showed that over half of the VEGF$^+$ cells co-expressed Flt1 (Fig. 2D, H). VEGF extensively co-labeled with S100β (Fig. 2G, H) but not with βIII-tubulin (Fig. 2G). Some BrdU$^+$ cells, mainly in ventral SVZa, were double-labeled for VEGF (Fig. 2F, H), and VEGF immunoreactivity was also found in the rostral migratory stream, on astrocytes (data not shown). The percentage of VEGF/BrdU co-labeling was significantly lower that the percentage of Flt1/BrdU co-labeling (Kruskal-Wallis Test, $P=0.006$).

Kit was expressed by astrocytes and progenitors

Immunostaining for Kit showed numerous positive cells with subependymal localization (Fig. 3A), and the Kit immunoreactivity did not extend in the rostral migratory stream (data not shown). Under higher magnification, the Kit$^+$ cells exhibited stellate morphology and were single cells not clusters (Fig. 3B). Kit did not co-label with βIII-tubulin (Fig. 3C), while it co-stained extensively with S100β (Fig. 3D, G). A small fraction of the Kit$^+$ cells were double-labeled for Flt1 (Fig. 3E), and an even smaller population of Kit$^+$ cells was positive for BrdU (Fig. 3F).

The expression in SVZa of the hematopoietic/angiogenic tyrosine kinase receptors Tie2 and Tie1, and the Tie2 ligands Ang-1 and -2 was restricted to endothelial cells (Fig. 3H–J).

The neurotrophins and their receptors in SVZa

Both the NGF (Fig. 4A) and BDNF (Fig. 4D) signals formed an immunopositive band of cells with subependymal localization, similarly to what observed for VEGF. NGF co-labeled with S100β (Fig. 4B) and with VEGF (Fig. 4C) but not with βIII-tubulin or BrdU (Fig. 4A, L). Similarly to NGF, BDNF exhibited a high percentage of co-labeling with S100β (Fig. 4D, M) but not with βIII-tubulin (Fig. 4E), and was also expressed in the rostral migratory stream (data

not shown). Both TrkA and TrkB co-labeled with S100β (Fig. 4F, N, O) and VEGF (Fig. 4I), but had a differential co-labeling pattern with BrdU and βIII-tubulin. TrkA was not expressed by the BrdU$^+$ clusters (Fig. 4G), while TrkB did co-stain with BrdU (Fig. 4H). TrkA was expressed in βIII-tubulin$^+$ cells (Fig. 4J) while TrkB was not co-stained with βIII-tubulin (Fig. 4O). Both TrkA and TrkB were present in the rostral migratory stream. The expression of the pan-neurotrophin receptor p75 was restricted to blood vessels (Fig. 4K).

The NT3/TrkC and the GDNF/glial cell line-derived neurotrophic factor family receptor α1 (GFRα1) neurotrophin systems had a comparable SVZa distribution. Double-staining for NT3 and its high-affinity receptor TrkC showed a prominent signal at the ependymal border (Fig. 5A1) although subependymal cells were stained as well (Fig. 5A2, A3). Neither NT3 nor TrkC did co-stain with BrdU (Fig. 5B). NT3 co-labeled with S100β (Fig. 5C, H1), and VEGF (Fig. 5D, H1), the double-stained cells exhibiting stellate morphology (Fig. 5C, D; arrows) or being perivascular. Further, NT3 co-stained with subependymal cells positive for GFRα1, the glycosylphosphatidylinositol-anchored cell surface receptor of GDNF (Fig. 5E). Most of the GFRα1$^+$ cells co-expressed S100β (Fig. 5H3), and a comparable percentage of GFRα1$^+$ cells were co-labeled for VEGF (Fig. 5F, H3). A comparison of the expression of GFRα1 with that of its ligand GDNF revealed that the in contrast to GFRα1, the GDNF immunoreactivity was mainly localized to the ependymal cells (Fig. 5G). Both GDNF and GFRα1 were also positive in SVZa blood vessels (Fig. 5G2, 5G3; arrows). Ret, the transmembrane tyrosine kinase receptor of GDNF was not expressed in SVZa.

DISCUSSION

In this study, we provided structural evidence that several angiogenic and/or neurotrophic factor systems were expressed at protein level in adult monkey progenitor cell niche. These ligand/receptor systems might be involved in the *in vivo* regulation of primate progenitor cells, and thus could be a feasible target for manipulation in precursor cell-centered therapies in humans. Further, our data represent an attempt to construct molecular phenotypization of the cellular types in the monkeys SVZa niche in order to better understand their interrelationships.

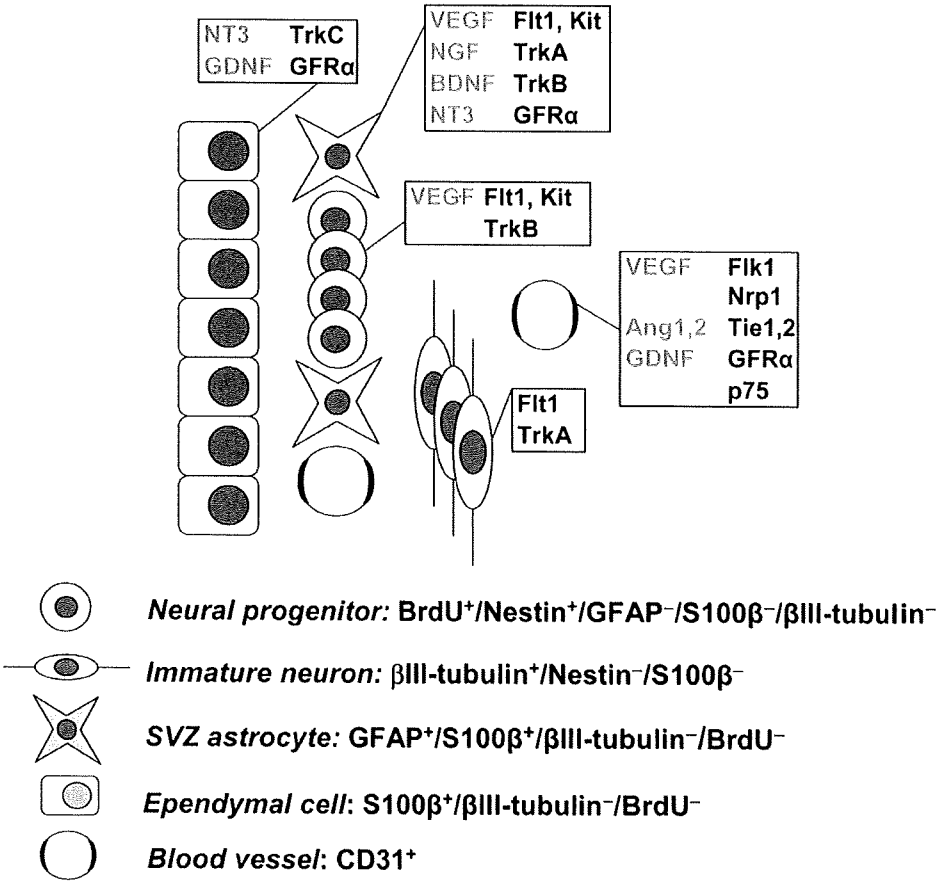

Fig. 6. Summary of ligand/receptor protein expression patterns by the major cell populations comprising monkey SVZa. Putative progenitor phenotypes are annotated in gray with their characteristic cell-selective marker combinations listed. Abbreviations: p75NTR, 75 kD pan-neurotrophin receptor.

We identified the characteristic expression pattern of angiogenic/neurotrophic signaling molecules and their receptors in five distinct cell types comprising the progenitor cell niche of adult monkey SVZa (Fig. 6). A link between blood vessels and neurogenesis is well appreciated in non-primate mammals (Leventhal et al., 1999; Palmer et al., 2000; Palmer, 2002; Louissaint et al., 2002; Shen et al., 2004; Wurmser et al., 2004), and begins to be unveiled in the monkey brain (Yamashima et al., 2004). The data presented in this study are in accordance with the view of a vascular signaling network involvement in primate progenitor cell regulation. Such a network could entail a neurotrophin–VEGF interplay, as $TrkA^+$ and $Flt1^+$ cells co-expressed VEGF, NGF and BDNF, opening a possibility for VEGF/neurotrophin paracrine or autocrine signaling (Calza et al., 2001; Louissaint et al., 2002; Fabel et al., 2003) in monkey SVZa. Further, SVZa astrocytes were positive for many of the molecules studied, and future studies are needed to delineate whether SVZa astrocytes are the principal progenitors in adult monkey SVZa (Sanai et al., 2004) or they are a non-progenitor cell type implicated in the regulation of the $BrdU^+$ precursors. Our results also suggest that ependyma-derived signals such as NT3 and GDNF could affect the subependymal niche cellular components in the monkey. In ischemic rodent brain, GDNF enhanced the SVZa progenitor neurogenesis (Kobayashi et al., 2006) via effects which do not appear to depend on the Ret tyrosine kinase (Arvidsson et al., 2001), consistent with the lack of Ret expression in SVZa in our monkey specimens. Thus, the operation of the GDNF system in SVZa may be exerted through GFRa1 and polysialylated neural cell adhesion molecule (PSA-NCAM) (Paratcha et al., 2006) signaling, or via additional transmembrane effectors (Pozas and Ibanez, 2005).

While the involvement of a vascular signaling network in the progenitor cell biology appears to be a conserved phenomenon between non-primate and primate mammals, interspecies molecular distinctions appear to exist. A major finding of the present study was the expression of the VEGF receptor Flt1 by proliferating progenitors of monkey SVZa, in contrast to the rodent SVZa where the major VEGF receptor expressed in the niche was Flk1 (Jin et al., 2002a). Notably, the Flt1-selective ligand VEGF-B also has pro-neurogenic effects in rodents (Sun et al., 2006), although of a significantly lower magnitude than the VEGF/Flk1-mediated effects (Jin et al., 2002a). The number of $Flt1^+/BrdU^+$ cells in monkey SVZa increased early after ischemia, while Flt1 was not present on the fraction of sustained progenitors remaining in SVZa for months after injury. These results suggest that Flt1 may be involved in the regulation of proliferation rather than differentiation of monkey precursor cells. Differential expression of Flt1, Flk1 and Nrp1 by primate or rodent precursors might be at least in part responsible for interspecies differences in progenitor cell biology (Sanai et al., 2004; Tonchev et al., 2003, 2005; Yamashima et al., 2004).

Deciphering the signaling regulating endogenous progenitor cell proliferation and differentiation in the primate brain is a requirement for developing effective cell replacement therapies in humans. The mere morphological finding of expression of a certain factor by a given cell type does not provide information on the function of this factor, and thus at present it remains unclear how the molecules investigated in our study would modulate monkey SVZa progenitors after ischemia or whether these factors are induced in response to the changes in the precursor cell proliferation and/or differentiation. Nevertheless, the results presented here are a step in determining the molecular "signature" of the cell types comprising monkey progenitor cell niche, and therefore may be helpful to more effectively design growth factor-based strategies for enhancement of endogenous precursor cells in monkey models, and eventually in the diseased human brain.

Acknowledgments—Research was sponsored by grants from the Japanese Ministries of Education, Culture, Sports, Science and Technology (Kiban B: 15390432) and Health, Labor and Welfare (H15-Kokoro-018), and the National Science Fund of Bulgaria (L1311/03). The technical expertise of Masaya Ueno is highly appreciated.

REFERENCES

Arvidsson A, Kokaia Z, Airaksinen MS, Saarma M, Lindvall O (2001) Stroke induces widespread changes of gene expression for glial cell line-derived neurotrophic factor family receptors in the adult rat brain. Neuroscience 106:27–41.

Arvidsson A, Collin T, Kirik D, Kokaia Z, Lindvall O (2002) Neuronal replacement from endogenous precursors in the adult brain after stroke. Nat Med 8:963–970.

Bedard A, Gravel C, Parent A (2006) Chemical characterization of newly generated neurons in the striatum of adult primates. Exp Brain Res 170:501–512.

Benraiss A, Chmielnicki E, Lerner K, Roh D, Goldman SA (2001) Adenoviral brain-derived neurotrophic factor induces both neostriatal and olfactory neuronal recruitment from endogenous progenitor cells in the adult forebrain. J Neurosci 21:6718–6731.

Calza L, Giardino L, Giuliani A, Aloe L, Levi-Montalcini R (2001) Nerve growth factor control of neuronal expression of angiogenetic and vasoactive factors. Proc Natl Acad Sci U S A 98:4160–4165.

Calza L, Giuliani A, Fernandez M, Pirondi S, D'Intino G, Aloe L, Giardino L (2003) Neural stem cells and cholinergic neurons: regulation by immunolesion and treatment with mitogens, retinoic acid, and nerve growth factor. Proc Natl Acad Sci U S A 100: 7325–7330.

Carmeliet P (2003) Blood vessels and nerves: common signals, pathways and diseases. Nat Rev Genet 4:710–720.

Chen Y, Ai Y, Slevin JR, Maley BE, Gash DM (2005) Progenitor proliferation in the adult hippocampus and substantia nigra induced by glial cell line-derived neurotrophic factor. Exp Neurol 196:87–95.

Dempsey RJ, Sailor KA, Bowen KK, Tureyen K, Vemuganti R (2003) Stroke-induced progenitor cell proliferation in adult spontaneously hypertensive rat brain: effect of exogenous IGF-1 and GDNF. J Neurochem 87:586–597.

Emanueli C, Schratzberger P, Kirchmair R, Madeddu P (2003) Paracrine control of vascularization and neurogenesis by neurotrophins. Br J Pharmacol 140:614–619.

Fabel K, Fabel K, Tam B, Kaufer D, Baiker A, Simmons N, Kuo CJ, Palmer TD (2003) VEGF is necessary for exercise-induced adult hippocampal neurogenesis. Eur J Neurosci 18:2803–2812.

Ferrara N, Gerber HP, LeCouter J (2003) The biology of VEGF and its receptors. Nat Med 9:669–676.